A Modeling Approach to Investigate Drivers, Variability and Uncertainties in O_2 Fluxes and O_2:CO_2 Exchange Ratios in a Temperate Forest

Yuan Yan[1], Anne Klosterhalfen[1], Fernando Moyano[1], Matthias Cuntz[2], Andrew C. Manning[3], Alexander Knohl[1,4]

[1] Bioclimatology, University of Goettingen, 37077 Goettingen, Germany
[2] Université de Lorraine, AgroParisTech, INRAE, UMR Silva, 54000 Nancy, France
[3] Centre for Ocean and Atmospheric Sciences, School of Environmental Sciences, University of East Anglia, Norwich, NR4 7TJ, United Kingdom
[4] Centre of Biodiversity and Sustainable Land Use (CBL), University of Goettingen, 37073 Goettingen, Germany

Correspondence to: Yuan Yan (yuanyantwincities@gmail.com)

Abstract. The O_2:CO_2 exchange ratio (ER) between terrestrial ecosystems and the atmosphere is a key parameter for partitioning global ocean and land carbon fluxes. The long-term terrestrial ER is considered to be close to 1.10 moles of O_2 consumed per mole of CO_2 produced. Due to the technical challenge in measuring directly the ER of entire terrestrial ecosystems (ER_{eco}), little is known about variations in ER at hourly and seasonal scales as well as how different components contribute to ER_{eco}. In this modeling study, we explored the variability and drivers of ER_{eco} and evaluated the hypothetical uncertainty in determining ecosystem O_2 fluxes based on current instrument precision. We adapted the one-dimensional, multi-layer atmosphere-biosphere gas exchange model, CANVEG, to simulate hourly ER_{eco} from modeled O_2 and CO_2 fluxes in a temperate beech forest in Germany.

We found that the modeled annual mean ER_{eco} ranged from 1.06 to 1.12 mol mol^{-1} within the five-years study period. Hourly ER_{eco} showed strong variations over diel and seasonal cycles and within the vertical canopy profile. Determination of ER from O_2 and CO_2 mole fractions in air above and within the canopy (ER_{conc}) varied between 1.115 and 1.15 mol mol^{-1}. CANVEG simulations also indicated that ecosystem O_2 fluxes could be derived with the flux-gradient method using measured vertical gradients in scalar properties, as well as fluxes of CO_2, sensible heat, and latent energy derived from eddy-covariance measurements. Owing to measurement uncertainties, however, the uncertainty in estimated O_2 fluxes derived with the flux-gradient approach could be as high as 15 µmol m^{-2} s^{-1}, which represented the 90% quantile of the uncertainty in hourly data with a high-accuracy instrument. We also demonstrated that O_2 fluxes can be used to partition net CO_2 exchange fluxes into their component fluxes of photosynthesis and respiration, if ER_{eco} is known. The uncertainty of the partitioned gross assimilation ranged from 1.43 to 4.88 µmol m^{-2} s^{-1} assuming a measurement uncertainty of 0.1 or 2.5 µmol m^{-2} s^{-1} for net ecosystem CO_2 exchange and from 0.1 to 15 µmol m^{-2} s^{-1} for net ecosystem O_2 exchange, respectively. Our analysis suggests that O_2 measurements at ecosystem scale have the potential for partitioning net CO_2 fluxes into their component fluxes, but further improvement in instrument precision is needed.

1 Introduction

Fluxes of O_2 and CO_2 between the terrestrial biosphere and atmosphere are inversely linked in photosynthesis, which
assimilates CO_2 and releases O_2, and in respiration, which consumes O_2 and releases CO_2 (Keeling and Manning, 2014; Keeling
and Shertz, 1992a; Krogh, 1919; Severinghaus, 1995). The relationship between these opposing fluxes can be described with
the so-called O_2:CO_2 exchange ratio (ER, see Table A1 in the Appendix for an overview of all abbreviations and variable
names used here), which should be considered on various temporal and spatial scales – ranging from hourly to decadal scales
temporally and from leaf to global scales spatially, respectively. Since the relationship of O_2 and CO_2 fluxes between the
atmosphere and different carbon reservoirs (terrestrial biosphere, oceans and fossil fuels) differ on regional and global scales,
these different ERs can be applied as parameters in global models in conjunction with observations of atmospheric O_2 and CO_2
abundances to quantify the global sinks of CO_2 into the ocean and the terrestrial biosphere (Battle et al., 2000; Ishidoya et al.,
2012; Keeling and Manning, 2014; Keeling and Shertz, 1992b; Tohjima et al., 2019). The global ER for the terrestrial biosphere
is commonly set to 1.10 moles of O_2 consumed per mole of CO_2 produced (or vice versa) (Severinghaus, 1995) by assuming
that this value, derived from elemental abundance data, is a representative long-term average for all land biota (Keeling and
Manning, 2014; Manning and Keeling, 2006). An ER of 1.05 mol mol^{-1} was determined by Randerson et al. (2006) based on
observed chemical compositions of plant parts for quantification of the global carbon sink. Measurements using the oxidative
ratio of organic material provided a more recent terrestrial ER estimate of 1.04 ± 0.03 mol mol^{-1} (Worrall et al., 2013). Using
an ER of 1.05 mol mol^{-1} instead of 1.10 mol mol^{-1} in carbon budget models will attribute 0.05 Pg C yr^{-1} more to the global
land carbon sink and an equivalent amount less to the ocean carbon sink (Keeling and Manning, 2014), indicating that the ER
needs to be well constrained when parameterized in global ocean and land carbon cycle models.

On ecosystem-scale, a mole fraction-based and a flux-based O_2:CO_2 ratio can be considered (Ishidoya et al., 2013; Seibt et al.,
2004). The former is defined as the fluctuations in the mole fraction of O_2 per mole fraction of CO_2 in the atmosphere (ER$_{conc}$).
Thus, ER$_{conc}$ is usually derived from the slopes of linear regressions between observed atmospheric O_2 and CO_2 mole fractions
(Battle et al., 2019; Ishidoya et al., 2013; Seibt et al., 2004). Battle et al. (2019) observed an average ER$_{conc}$ = 1.08 ± 0.007 mol
mol^{-1} in a mixed deciduous forest over a six-years period with temporal variations on a 6-hour basis ranging between 0.85 and
1.15 mol mol^{-1}. Measurements of canopy air O_2 and CO_2 mole fractions at two different forest sites yielded ER$_{conc}$ estimations
between 1.01 and 1.03 mol mol^{-1} averaged over 24-hour periods and between 1.14 and 1.19 mol mol^{-1} during daytime only
(Seibt et al., 2004). Ishidoya et al. (2013) obtained differing ER$_{conc}$ at two heights within a cool temperate deciduous forest,
reflecting variations of ER$_{conc}$ with canopy height. Furthermore, they observed different ER$_{conc}$ during daytime (0.87 mol mol^{-1}) and nighttime (1.03 mol mol^{-1}) in summer, indicating a significant variation of ER$_{conc}$ over the diel period (Ishidoya et al.,
2013). Faassen et al. (2022) found much higher ER$_{conc}$ over 24 hours (2.05 ± 0.03 mol mol^{-1}) than for daytime only (1.10 ±
0.12 mol mol^{-1}) and nighttime only (1.22 ± 0.02 mol mol^{-1}) due to variations in the boundary layer height during the
measurement period.

65   The flux-based O_2:CO_2 ratio is defined as the O_2 flux per CO_2 flux between an ecosystem and the atmosphere (ER_{eco}). Flux estimates can be described as the net turbulent exchange or the overall net exchange (turbulent plus storage flux), where we focused on the latter in this study. Very few studies have attempted to quantify ER_{eco} because measuring O_2 fluxes at ecosystem scale is still a major challenge. Since O_2 and CO_2 are strongly anti-correlated in the processes of photosynthesis and respiration, changes in both scalars are very similar in absolute numbers, typically in the order of a few ppm. However, the relative changes

70   in O_2 are much smaller than in CO_2 owing to the much higher atmospheric abundance (around 210,000 ppm for O_2 and around 400 ppm for CO_2), making O_2 measurements at sufficient precision and accuracy technically challenging. Thus, previous studies resorted to, for instance, the flux-gradient method, chamber measurements and modeling approaches. Ishidoya et al. (2015) determined a daily mean net turbulent ER = 0.86 mol mol^{-1} based on O_2 and CO_2 gradient measurements. Faassen et al. (2022) reported daytime and nighttime ER_{eco} as 0.92 ± 0.17 and 1.03 ± 0.05 mol mol^{-1}, respectively. In general, ER_{eco}

75   depends on the elemental composition and reduction state of organic material, and on the temporal variation and spatial distribution of sinks and sources of ecosystem flux components (Seibt et al., 2004). As described by Battle et al. (2019), the dynamics and interrelations of the various sinks and sources within the ecosystem, each with their own ER_{eco}, result in the mixed signal ER_{conc}.

    Current micrometeorological approaches to measure gas exchange between ecosystems and the atmosphere include eddy

80   covariance, flux-gradient and eddy accumulation methods, which could all theoretically be used to determine ecosystem O_2 fluxes. The applicability of the eddy covariance technique for O_2 flux estimation, however, requires high precision at a high measurement frequency (10-20 Hz). Except for a homemade, non-commercial vacuum ultraviolet (VUV) absorption analyzer (Stephens et al., 2003) no suitable instrument exists so far. The application of the eddy accumulation method is also technically challenging and has not yet been applied to O_2 (Emad and Siebicke, 2023a, b).

85   With the flux-gradient method, O_2 fluxes can be inferred from an O_2 gradient above a canopy and from an eddy diffusivity (K), which can be derived based on additional CO_2, sensible or latent heat flux measurements (Baldocchi et al., 1988). This method assumes that heat and mass are transported in a similar manner between two adjacent levels above the canopy (Baldocchi et al., 1988). The method's applicability is again particularly challenging for O_2 estimates owing to the typically large measurement uncertainty in relation to the small O_2 gradient. One approach to increase the measurement-to-noise ratio

90   is to move the lower inlet of the gradient measurement closer to or even inside the canopy. This approach, however, violates the assumption of the flux-gradient method owing to infrequent but predominantly large eddies within the canopy, counter-gradient fluxes and possible non-differentiable gradients (Raupach, 1989; Wilson, 1989). The flux-gradient method has already been used for O_2 flux estimation above a cool temperate forest (Ishidoya et al., 2015), an urban canopy (Ishidoya et al., 2020) and a boreal forest (Faassen et al., 2022). The theoretical limits of the flux-gradient method for O_2 fluxes given current

95   instrument precision and accuracy are, however, not yet fully explored.

    Chamber level gas exchange measurements provide an alternative approach to measure the ER of individual components such as leaf, stem and soil, which could be scaled up to ecosystem level. Branch and soil chamber measurements in a German temperate forest showed an average ER of leaf net assimilation (ER_{An}; net assimilation defined as carboxylation minus

photorespiration and dark respiration) between 1.08 ± 0.16 mol mol^{-1} and 1.19 ± 0.12 mol mol^{-1}, and an ER of soil respiration

100 (ER$_{soil}$) of 0.94 ± 0.04 mol mol^{-1} (Seibt et al., 2004). In a cool temperate deciduous forest in Japan, chamber measurements indicated an ER$_{An}$ = 1.02 ± 0.03 mol mol^{-1} and ER$_{soil}$ = 1.11 ± 0.01 mol mol^{-1} (Ishidoya et al., 2013). Hilman et al. (2019) measured an average ER of stem respiration (ER$_{stem}$) between 0.97 and 1.95 mol mol^{-1} for tropical, temperate and Mediterranean trees with a closed-flow chamber system with two continuous flow analyzers.

The ER variability in assimilation and respiration fluxes found in these studies provides a potential approach to partition net

105 CO_2 fluxes into their components following similar approaches based on stable isotopes in CO_2 (Knohl and Buchmann, 2005; Ogee et al., 2004; Wehr and Saleska, 2015; Zobitz et al., 2007). Using simultaneous measurements of net ecosystem O_2 and CO_2 fluxes and considering the ER for the photosynthetic and respiratory processes in a canopy and at the soil surface, two mass balance equations can be written for O_2 and CO_2 (see Eq. (1) below). Hourly or half-hourly ER would be needed to agree with the typical time step of flux estimates derived with the eddy covariance technique, which is the standard method of

110 measuring gas exchange between land surfaces and the atmosphere (Baldocchi et al., 2001; Goulden et al., 1996). Theoretically, such an O_2-based partitioning method only works for periods when the ER of gross assimilation (ER$_A$) and gross ecosystem respiration (ER$_R$) differ, because a second independent mass balance equation is needed to yield CO_2 fluxes of assimilation (F$_A$) and respiration (F$_R$). According to Ogee et al. (2004), the difference in ER has to be large enough to obtain a reasonable accuracy in the partitioned net CO_2 fluxes. Consequently, an analysis of temporal dynamics in ER$_A$ and ER$_R$ is

115 necessary in order to evaluate the possibility of applying O_2 observations in a CO_2 flux partitioning approach.

The contribution of flux components to the temporal and spatial variability on overall ecosystem O_2 fluxes can also be explored by modeling approaches. For example, net turbulent ER was simulated with a simple one-box model with daily time steps, by assuming that O_2 and CO_2 mole fractions are spatially constant and temporally variable within the canopy (Ishidoya et al., 2015; Seibt et al., 2004). These simulations indicated that variations in net turbulent ER are not only influenced by leaf and

120 soil fluxes, but also by turbulence inside and outside the canopy (Seibt et al., 2004). To explore the drivers of ER variations at the ecosystem scale, more precise turbulence effects need to be considered. However, simple one-box models assume uniform and well-mixed air columns throughout the canopy, so that modeled ER lacks variations for different layers within the canopy.

Multi-layer atmosphere-biosphere models such as CANVEG (Baldocchi, 1997; Baldocchi and Wilson, 2001) differ from one-box models in that they are designed to represent the temporal and (vertical) spatial scale of an eddy covariance tower.

125 Therefore, they are a good simulator to test and examine new types of observations (Oikawa et al., 2017). CANVEG includes within-canopy transport of CO_2, water vapor and energy (Baldocchi, 1997; Baldocchi and Wilson, 2001), so that if it were adapted to O_2 processes, one could evaluate the accuracy of different flux measurement techniques such as eddy covariance or flux-gradient approaches. Published ER values of gross and/or net assimilation, stem respiration and soil respiration can be employed as parameters to derive component-specific O_2 fluxes from existing modeled CO_2 fluxes. Thus, concurrent O_2 and

130 CO_2 fluxes, and ER can be plausibly simulated for multiple canopy layers and for the whole ecosystem, with which we can analyze the main drivers of modeled ER values, their diel and seasonal variability, and vertical variations. In addition, concurrently simulated mole fraction profiles – a function of turbulent dispersion and the strength and location of scalar sources

and sinks – enable us to test the precision of the flux-gradient method for O_2 flux estimation while choosing various measurement heights inside and above the canopy. Furthermore, the performance of an O_2-based source partitioning method can be evaluated based on model simulations.

Given these considerations, we defined the following objectives for this study: (1) to implement atmosphere-biosphere O_2:CO_2 exchange ratios for various ecosystem components in the multi-layer CANVEG model; (2) to explore temporal and spatial variations in O_2:CO_2 exchange ratios at ecosystem scale as well as the underlying main ; (3) to evaluate the potential precision of the flux-gradient approach to obtain O_2 fluxes; and (4) to evaluate the feasibility of O_2 flux measurements for CO_2 flux partitioning.

2 Methods

2.1 Site description

The meteorological and plant-specific ecophysiological measurements used in our model simulation were derived from the Leinefelde FLUXNET tower site (DE-Lnf, https://doi.org/10.18140/FLX/1440150) located in central Germany (51°19′42”N, 10°22′04”E, 450 m a.s.l.; (Anthoni et al., 2004)). The vegetation at the site is an even-aged managed beech stand (*Fagus sylvatica* L.) with an age of approximately 130 years (Tamrakar et al., 2018). Between 2002 and 2016, the mean annual temperature was 8.3 ± 0.7 °C and the average cumulative annual precipitation was 600 ± 150 mm (Braden-Behrens et al., 2019). The canopy height (ht) was 37.5 m and the effective leaf area index (LAI) was at maximum 4.8 m^2 m^{-2} in the growing season in 2015 (Braden-Behrens et al., 2017).

Meteorological variables are continuously measured including air temperature, air humidity, direct and diffuse global radiation, photosynthetic photon flux density, wind velocity, air pressure, vapor pressure deficit, precipitation, atmospheric CO_2 mole fraction ($CO_{2\ atm}$), soil temperature and soil moisture. Also, fluxes of net ecosystem CO_2 exchange (F_{CO_2}), sensible heat (H), and latent heat (LE) are obtained with the eddy covariance technique at 44 m above the ground level (Anthoni et al., 2004). The meteorological variables were used as input data for our model simulations, while the flux estimates were storage-term corrected and then used for model calibration and validation (see below). In this paper, upward fluxes (release to the atmosphere) are presented as positive quantities and downward fluxes (uptake by the ecosystem) as negative quantities. Thus, O_2 fluxes always have opposite signs to their corresponding CO_2 fluxes, which is in line with micrometeorological conventions.

2.2 Model description and model set-up

We used the one-dimensional, multi-layer atmosphere-biosphere gas exchange model, "CANVEG", described by Baldocchi (1997) and Baldocchi and Wilson (2001). The model domain included 120 model layers above the ground, in which the lower 40 above-ground layers covered the entire canopy, while the bottom layer represented the soil surface for the description of soil carbon and energy fluxes. The domain also included 10 below-ground soil layers; however, this study did not consider

processes within the soil column in any detail. CANVEG used hourly meteorological variables as drivers, as well as site-specific parameters (see Table 1) to simulate biosphere-atmosphere water vapor, CO_2 and energy fluxes within and above the forest canopy.

The carbon, water and energy modules in CANVEG have been validated for various environmental conditions and forest types (Baldocchi, 1997; Baldocchi et al., 2002; Baldocchi et al., 1999). Moreover, CANVEG has previously been applied to an unmanaged beech-dominated forest site only 30 km away from the site of this study (Knohl and Baldocchi, 2008), and has recently been used to simulate the isotopic composition of carbon assimilates at Leinefelde (Braden-Behrens et al., 2019). We translated the original C code (Baldocchi, 1997) to Fortran 90, which was then used for further implementations.

Atmospheric O_2 mole fraction ($O_{2\ atm}$) as an input for the model was deduced from a fixed O_2:CO_2 mole ratio of -1.15 mol mol^{-1} and continuous CO_2 mole fraction measurements at the site (Table 1). The fixed O_2:CO_2 mole ratio was derived from measurements at the University of Göttingen from November 2017 to January 2018 using a high-precision O_2 measurement system developed by Dr. Penelope Pickers (University of East Anglia, UK) and very similar to the system described in Pickers et al. (2017). For these measurements, the correlation between O_2 and CO_2 mole fractions had an $R^2 = 0.99$.

Some model parameters regarding leaf photosynthesis, stomatal conductance and soil respiration were fitted to the actual site conditions via the Markov Chain Monte Carlo (MCMC) method (Van Oijen et al., 2005). Eddy covariance measurements of hourly F_{CO_2}, H and LE, and the estimated ecosystem respiration (F_R) in 2012 and 2013 were used to calibrate the model parameters (

Table 1). The years 2014-2016 were used for model validation. The leaf phenology parameters, including day of year (DOY) for the start of leaf growth, end of leaf growth, start of leaf fall and end of leaf fall (leaf$_{out}$, leaf$_{full}$, leaf$_{fall}$, and leaf$_{fall\_complete}$) were derived from daily camera images in 2015 above the canopy. LAI during the course of a year was simulated based on these four parameters: the DOY range before leaf$_{out}$ and after leaf$_{fall\_complete}$ was defined as winter, when LAI = zero, and the DOY range between leaf$_{full}$ and leaf$_{fall}$ was defined as summer when LAI = 4.8 m^2 m^{-2}. During spring (leaf$_{out}$ < DOY < leaf$_{full}$) and during autumn (leaf$_{fall}$ < DOY < leaf$_{fall\_complete}$) LAI increased or decreased linearly, respectively. The maximum LAI of 4.8 m^2 m^{-2} as well as the LAI fraction (f_{LAI}) at five different heights in the canopy were measured using a LI-2000 plant canopy analyzer (LI-COR Biosciences GmbH, Germany) in 2015 (Braden-Behrens et al., 2017). The vertical LAI profile was assumed to follow a beta-distribution, which was fitted to the observed f_{LAI} (Table 1). This relationship between LAI and height (z) allocates leaves mainly in the upper canopy (z/ht $\geq$ 0.45) with almost no leaves in the bottom canopy (Fig. 1a). The wood area index (WAI) consisted of the branches (80% of total WAI) and the stems (20% of total WAI). The branches were situated in the upper canopy (z/ht $\geq$ 0.45) following the same distribution algorithm as LAI, while in the lower canopy (z/ht < 0.45), the fraction of stem WAI per layer to total stem area was deduced from the fraction of stem diameter per layer to the diameter at breast height (f_{DBH}) as a function of height (z): $f_{DBH} = 102 - 2.6z + 0.08z^2 - 0.0023z^3$ (Schober, 1952). This set-up of the forest canopy including leaf phenology and the vertical LAI and WAI profiles were used for all years of the model run. All site-specific parameters used in this study are listed in Table 1.

For the simulation of net ecosystem O_2 fluxes (F_{O_2}), values of ER had to be chosen: the input parameter of ER_A was set to 1.00 mol mol^{-1} (Table 1), by assuming that photosynthesis produces glucose ($C_6H_{12}O_6$), resulting in equal O_2 and CO_2 fluxes. The ER of canopy respiration was attributed to the ER of leaf dark respiration (ER_{rd}) and stem respiration (ER_{stem}). ER_{stem} was fixed to 1.04 mol mol^{-1} (Randerson et al., 2006), while the ER_{rd} was set to increase with leaf temperature (T_{leaf}; Fig. 1b) according to Tcherkez et al. (2003). ER_{soil} was set to 1.10 mol mol^{-1} (Randerson et al., 2006; Severinghaus, 1995). To quantify the dependency of the CANVEG model regarding these fixed ER parameters, we also conducted a sensitivity analysis, where we changed each of ER_A, ER_{stem} and ER_{soil} by ±10% and estimated the resulting relative changes in simulated O_2 fluxes. Furthermore, the impact of changed ER parameters was also investigated in the following parts of this study (see sections 2.3 and 2.5 below).

To validate the model, we used eddy covariance measurements of F_{CO_2}, H and LE from 2014 to 2016. To quantify the model performance, we calculated the slope, intercept, and the coefficient of determination (R^2) of a linear regression between modeled and observed F_{CO_2}, H and LE, as well as the root mean square error (RMSE).
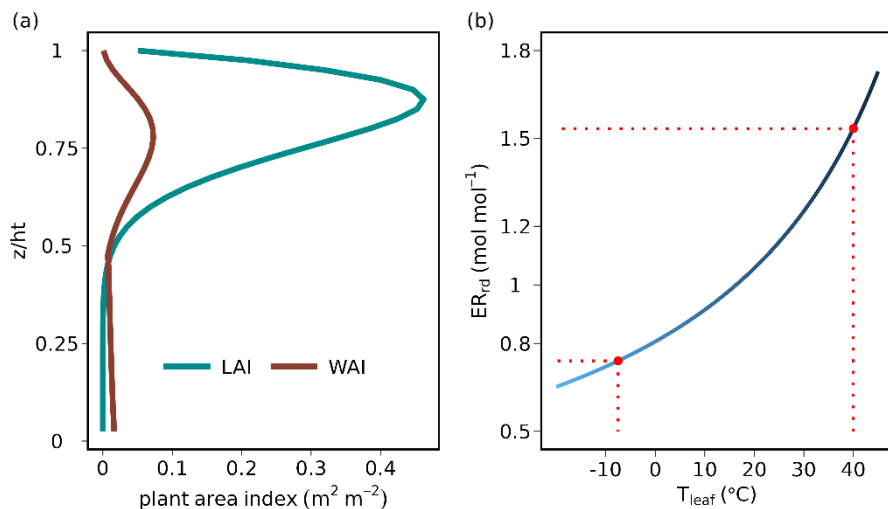
Figure 1. (a) Distribution of vertical leaf and wood area indices (LAI and WAI in m^2 m^{-2} per canopy layer) used in the CANVEG model, derived from measurements at the Leinefelde study site (Braden-Behrens et al., 2017). The y-axis is the ratio of the height in the canopy (z) to the top of the canopy (ht). (b) O_2:CO_2 exchange ratio of leaf dark respiration (ER_{rd} in mol mol^{-1}) as a function of leaf temperature (T_{leaf} in °C) after Tcherkez et al. (2003). The red dashed lines indicate the range of T_{leaf} and corresponding ER_{rd} in this study.

Table 1. Model parameters adjusted to the study site Leinefelde, Germany.

Parameter name	Details	Value
k_{ball}	slope of Ball-Berry model after Collatz et al. (1991)	10.4 [*]

b	intercept of Ball-Berry model after Collatz et al. (1991)	0.0014 µmol m^{-2} s^{-1} [*]
V_{cmax25}	maximum carboxylation at 25 °C	59.6 µmol m^{-2} s^{-1} [*]
R_{d25}	leaf dark respiration at 25 °C	$0.0149 \cdot V_{cmax25}$ [*]
J_{max25}	maximum electron transport rate at 25 °C	$2.24 \cdot V_{cmax25}$ [*]
θ_J	curvature parameter of light response curve	0.882 [*]
α	fraction of the photosystem II activity	0.284 [*]
r_1, r_2	coefficients for exponential relationship between soil temperature and soil respiration	0.827, 0.075 [*]
leaf$_{out}$	DOY for the start of leaf growth	110
leaf$_{full}$	DOY for the end of leaf growth	130
leaf$_{fall}$	DOY for the start of leaf fall	282
leaf$_{fall\_complete}$	DOY for the end of leaf fall	320
LAI	leaf area index	4.8 m^2 m^{-2}
f_{LAI}	fraction of LAI per layer	0, 0.04, 0.66, 0.2, 0.1 at 7.5, 17, 28, 32.5 and 37.5 m
O$_2$ atm	atmospheric O$_2$ mole fraction	O$_2$ atm = -1.15 CO$_2$ atm + 209749.5 (ppm)
ht	canopy height	37.5 m
ER$_A$	O$_2$:CO$_2$ exchange ratio of gross assimilation	1.00 mol mol^{-1}
ER$_{rd}$	O$_2$:CO$_2$ exchange ratio of leaf dark respiration depending on leaf temperature (°C)	$ER_{rd} = \frac{1}{-0.0147\ T_{leaf} + 1.24}$ (mol mol^{-1}) (Tcherkez et al., 2003)
ER$_{stem}$	O$_2$:CO$_2$ exchange ratio of stem respiration	1.04 mol mol^{-1} (Randerson et al., 2006)
ER$_{soil}$	O$_2$:CO$_2$ exchange ratio of soil respiration	1.10 mol mol^{-1} (Severinghaus, 1995)

[*] Parameters were calibrated with eddy covariance measurements of hourly F_{CO_2}, F_R, H and LE in 2012 and 2013 via the Markov Chain Monte Carlo (MCMC) method.

2.3. Model simulations of flux- and mole fraction-based exchange ratios

In CANVEG, CO$_2$ fluxes are simulated for the leaf, stem and soil components. The O$_2$ fluxes of each component are estimated by scaling each corresponding CO$_2$ flux by its ER. Respiratory CO$_2$ fluxes are defined to be positive, while assimilation CO$_2$ fluxes are negative. O$_2$ fluxes always have the opposite sign from the corresponding CO$_2$ fluxes, which would result in negative ER values. However, we have defined all ER parameters to be positive by including the factor (-1) in all relevant equations (see below), to be consistent with most published literature concerning O$_2$:CO$_2$ exchange ratios (Ishidoya et al., 2013; Seibt et al., 2004). Another way of considering this is that the ERs are the ratios of moles of O$_2$ consumed per mole of CO$_2$ produced (or moles of O$_2$ produced per mole of CO$_2$ consumed).

The O_2 and CO_2 ecosystem fluxes are the balance of the simulated fluxes of gross assimilation (F_A, carboxylation minus photorespiration) and gross ecosystem respiration (F_R). The latter consists of leaf dark respiration (F_{rd}), stem respiration (F_{stem}) and soil respiration (F_{soil}, consisting of 50% respiration by heterotrophs and 50% by autotrophs):

230
$$\begin{cases} F_{CO_2} = F_A + F_{rd} + F_{stem} + F_{soil} = F_A + F_R \\ F_{O_2} = -F_A \, ER_A - F_{rd} \, ER_{rd} - F_{stem} \, ER_{stem} - F_{soil} \, ER_{soil} = -F_A \, ER_A - F_R \, ER_R \end{cases} \quad (1)$$

where ER_A, ER_{rd}, ER_{stem} and ER_{soil} are given as model parameters (see Section 2.2.). The simulated F_{O_2} and F_{CO_2} include the storage fluxes associated with changes of O_2 and CO_2 mole fractions in the canopy air space, because they were inferred by integrating fluxes for all canopy layers. In general, the CANVEG model only considered dry mole fractions of O_2 and CO_2.

235 Usually, O_2 measurements are reported in per meg, which describes the change in the O_2 to N_2 ratio relative to a reference. To convert from ppm to per meg, the factor $1/0.2095 = 4.8$ per meg ppm^{-1} can be used, where 0.2095 represents the O_2 mole fraction of air in mol mol^{-1}. In this study, we chose mole fraction as unit for O_2 to be consistent in regard to the calculation of $O_2{:}CO_2$ exchange ratios, which are usually presented in mol mol^{-1}.

240 For the model simulations, ER could be obtained for the entire ecosystem, the net assimilation at the leaf level, or for only respiratory processes by considering the simulations of the corresponding flux components. The ER of the overall ecosystem (ER_{eco}) in hourly time steps was calculated as the ratio of the hourly F_{O_2} and F_{CO_2} (including storage terms) summed up over the entire canopy height, that is:

245
$$ER_{eco} = -\frac{F_{O_2}}{F_{CO_2}} \quad (2)$$

ER_{eco} for specific canopy heights (ER^z_{eco}) was derived as the slope of linear regressions fitted to O_2 and CO_2 fluxes of multiple simulated time steps for each canopy layer.

Furthermore, the simulated ER of net O_2 and CO_2 assimilation (ER_{An}) and of all respiratory fluxes (ER_R) were derived as:

250

$$ER_{A_n} = -\frac{-F_A \, ER_A - F_{rd} \, ER_{rd}}{F_A + F_{rd}} \quad (3)$$

$$ER_R = -\frac{-F_{rd} \, ER_{rd} - F_{stem} \, ER_{stem} - F_{soil} \, ER_{soil}}{F_{rd} + F_{stem} + F_{soil}} \quad (4)$$

Moreover, we assessed the impact of the model parameters ER_A, ER_{stem} and ER_{soil} by changing each by $\pm 10\%$ on estimates for
255 ER_{eco} and ER_{An} within the sensitivity analysis.

The atmospheric O_2 mole fraction at each canopy layer was also computed by CANVEG, analogous to that done for CO_2 mole fraction (Baldocchi, 1997). CANVEG estimated atmospheric mole fraction per layer as a function of multi-layer gas flux diffusion determined by a Lagrangian dispersion matrix (Baldocchi, 1992) and the atmospheric background gas mole fraction. The mole fraction-based ER (ER_{conc}) and ER_{conc} in specific canopy heights (ER^z_{conc}) were defined as the ratio between the fluctuations in O_2 and CO_2 mole fractions, and both were calculated as the slopes of linear regressions fitted to hourly atmospheric O_2 versus CO_2 mole fractions for the growing seasons (the days of year with leaves in the canopy, between $leaf_{out}$ and $leaf_{fall\_complete}$) of all simulation years (Battle et al., 2019; Ishidoya et al., 2013; Seibt et al., 2004). Thus, we obtained ER^z_{eco} and ER^z_{conc} with the same approach by deriving the slopes of hourly data to allow a comparison.

2.4. Evaluation of the flux-gradient method to obtain O_2 fluxes

The CANVEG simulations of ecosystem O_2 fluxes and O_2 mole fraction gradients provided the opportunity to test the applicability of the flux-gradient approach to estimate F_{O_2}. We assumed the flux-gradient measurement system could be installed both above the canopy and close to the forest floor. We especially aimed at testing the performance of the flux-gradient method based on current typical instrument performance for O_2 measurements. The turbulent O_2 ($F_{\widetilde{O_2}}$), CO_2 ($F_{\widetilde{CO_2}}$), sensible heat ($\widetilde{H}$) and latent heat ($\widetilde{LE}$) fluxes are related to vertical scalar gradients as follows (Meredith et al., 2014):

$$\begin{cases} F_{\widetilde{O_2}} = -K_o \frac{\Delta o}{\Delta z} \rho_n \\ F_{\widetilde{CO_2}} = -K_c \frac{\Delta c}{\Delta z} \rho_n \\ \widetilde{H} = -K_T \frac{\Delta T}{\Delta z} \rho_m c_p \\ \widetilde{LE} = -K_v \frac{\Delta v}{\Delta z} \lambda \end{cases} \tag{5}$$

where Δz (m) is the vertical height difference between the two measurement heights, ΔT, Δv, Δc and Δo denote the difference of air temperature (K), water vapor (kg m^{-3}), CO_2 dry air mole fraction (ppm) and O_2 dry air mole fraction (ppm) between measurement heights, respectively, ρ_n and ρ_m are the molar density (mol m^{-3}) and mass density of the air (kg m^{-3}), respectively, c_p is the specific heat capacity of air (J kg^{-1} K^{-1}), and λ is the latent heat of evaporation (J kg^{-1}). The superscript tilde in the flux nomenclatures denotes turbulent fluxes (without storage fluxes). K_o, K_c, K_T, and K_v (m^2 s^{-1}) are the eddy diffusivities of the relevant scalars. Assuming that heat and mass are transported in a similar way between two adjacent levels above the canopy and so assuming that $K_o=K_c=K_T=K_v$ (Baldocchi et al., 1988), then O_2 fluxes can be estimated with each of the following equations:

$$\begin{cases} F_{\widetilde{O_2},c} = F_{\widetilde{CO_2}} \dfrac{\Delta o}{\Delta c} \\[2mm] F_{\widetilde{O_2},T} = H^{\sim} \dfrac{\Delta o \, \rho_n}{\Delta T \, \rho_m \, c_p} \\[2mm] F_{\widetilde{O_2},v} = LE^{\sim} \dfrac{\Delta o \, \rho_n}{\Delta v \, \lambda} \end{cases} \tag{6}$$

From simulations of $F_{\widetilde{CO_2}}$, $H^{\sim}$ and $LE^{\sim}$ and vertical scalar profiles, we derived F_{O_2} from $F_{\widetilde{O_2}}$ plus the storage term based on the flux-gradient method and compared these to the directly modeled F_{O_2} (Eq. (1)). Here, the subscripts c, T and v denote which flux and scalar are used (CO_2 mole fraction, air temperature or water vapor, respectively).

There are usually three main sources of error in the flux-gradient method: (1) the uncertainty in the vertical gradient (that is, the gradient of O_2 mole fraction, $\frac{\Delta o}{\Delta z}$) resulting from the precision and accuracy of the measurement instruments, (2) the magnitude of the mole fraction difference (Δc, ΔT, or Δv) between the two measurement heights, which is usually small when the measurement heights are too close to each other or when the atmosphere is well mixed, and (3) the measurement uncertainty in the turbulent fluxes ($F_{\widetilde{CO_2}}$, $H^{\sim}$, or $LE^{\sim}$), which we assumed to be zero, because we applied here only our simulated turbulent fluxes. So here, we quantified the extent of the first two sources of uncertainty, and defined conditions when the flux-gradient method could perform satisfactorily to obtain F_{O_2}. The influence of the first uncertainty was evaluated by adding a "measurement error" to Δo, where the uncertainty was assumed to be normally distributed with a mean of zero and a standard deviation of ± 0.7 ppm (3.36 per meg), based on typical measurement uncertainty of the O_2 mole fraction instrument used to derive the fixed atmospheric O_2:CO_2 ratio (Pickers et al., 2017). Then the difference between the F_{O_2} derived via the flux-gradient method with and without the measurement uncertainty ($\sigma_{F_{O_2}}$) was evaluated.

The second uncertainty due to the magnitude in the gradient as a function of Δz was analyzed by estimating F_{O_2} based on the flux-gradient between a top measurement height at two times the canopy height in our model set-up and each layer below, until the soil surface (z/ht = 0). The top measurement height was set to z/ht = 2 following customary recommendations for the setup of eddy covariance towers following Rebmann et al. (2018). We also included measurement heights inside the canopy, where the vertical profiles are mostly non-linear due to scalar sources and sinks, to illustrate the effect of violating the assumptions of the flux-gradient method. For comparison, the difference between the F_{O_2} estimations derived by the flux-gradient method ($F_{\widetilde{O_2},(c,T,v)}$, based on $F_{\widetilde{CO_2}}$, $H^{\sim}$ or $LE^{\sim}$ and their respective vertical scalar profile) and by model simulations ($F_{\widetilde{O_2},CANVEG}$) was calculated:

$$\Delta F_{O_2,(c,T,v)} = F_{\widetilde{O_2},(c,T,v)} - F_{\widetilde{O_2},CANVEG} \tag{7}$$

where ΔF_{O_2} is the difference for the application between the top measurement height (z/ht = 2) and each layer below.

310 Finally, we also tested a three-heights flux-gradient method after the recent study of Faassen et al. (2022). They derived scalar concentrations at three heights (z/ht = 0.9, 3.7 and 6.9 with ht = 18 m), fitted a quadratic scalar-height relationship, and expressed the vertical gradient as the first derivative of z (see Eq. (10) and (11) by Faassen et al. (2022)). In our study, we selected the three heights at z/ht = 1.05, 1.45 and 2 with ht = 37.5 m, to be with all heights above the canopy.

2.5. Uncertainties in partitioning net ecosystem CO_2 fluxes based on O_2 fluxes

315 The net ecosystem CO_2 exchange (F_{CO_2}) consists of two different components: gross assimilation (F_A) and gross ecosystem respiration (F_R). Similar to the stable isotope flux partitioning approach (Bowling et al., 2001; Knohl and Buchmann, 2005; Ogee et al., 2004; Oikawa et al., 2017; Yakir and Wang, 1996), O_2 and CO_2 flux mass balance equations can be written as shown in Eq. (1), where F_{CO_2} is the observed ecosystem flux from eddy covariance measurements and F_{O_2} is obtained by multiplying F_{CO_2} by the modeled ER_{eco} in CANVEG following Eq. (2) (owing to the lack of actual F_{O_2} measurements). We

320 treated these mass balance equations as a probabilistic process assuming terms on the right-hand side are uncertainty quantities with *a priori* values (F_A^b, F_R^b, ER_A^b, ER_R^b) and uncertainties ($\sigma_{F_A^b}$, $\sigma_{F_R^b}$, $\sigma_{ER_A^b}$, $\sigma_{ER_R^b}$). Fluxes and exchange ratios, i.e. F_A, F_R, ER_A and ER_R, can be then calculated that minimize the differences between the left-hand side observations and the right-hand side "model" under consideration of their uncertainties, leading to *a posteriori* quantities (F_A, F_R, ER_A, ER_R) with corresponding uncertainties (σ_{F_A}, σ_{F_R}, σ_{ER_A}, σ_{ER_R}). A cost function (J) was then written as a linear system with all the differences weighted

325 by the corresponding *a priori* uncertainties:

$$J = \frac{1}{2}\left[\left(\frac{F_A+F_R-F_{CO_2}}{\sigma_{F_{CO_2}}}\right)^2 + \left(\frac{F_A\,ER_A+F_R\,ER_R-F_{O_2}}{\sigma_{F_{O_2}}}\right)^2 + \left(\frac{F_A-F_A^b}{\sigma_{F_A^b}}\right)^2 + \left(\frac{F_R-F_R^b}{\sigma_{F_R^b}}\right)^2 + \left(\frac{ER_A-ER_A^b}{\sigma_{ER_A^b}}\right)^2 + \left(\frac{ER_R-ER_R^b}{\sigma_{ER_R^b}}\right)^2\right] \quad (8)$$

The last four terms allow a solution to be defined with fewer equations than unknowns. The *a posteriori* values and

330 uncertainties were returned at minimum J with predefined *a priori* values and uncertainties (Table 2). For the J function with multiple variables as in our case, the *a posteriori* means of any parameter, x, were found along the gradient of each variable where its Jacobian equaled zero ($\frac{\partial J}{\partial x} = 0$; (Tarantola, 2004)), while the corresponding *a posteriori* uncertainties were expressed as the square root of the inverse Hessian at the minimum ($\frac{\partial^2 J}{\partial x^2}$; (Tarantola, 2004)):

335
$$\begin{bmatrix} \sigma_{F_A} \\ \sigma_{F_R} \\ \sigma_{ER_A} \\ \sigma_{ER_R} \end{bmatrix} = \sqrt{\begin{bmatrix} \frac{\partial^2 J}{\partial F_A^2} & \frac{\partial^2 J}{\partial F_A\,\partial F_R} & \frac{\partial^2 J}{\partial F_A\,\partial ER_A} & \frac{\partial^2 J}{\partial F_A\,\partial ER_R} \\ \frac{\partial^2 J}{\partial F_R\,\partial F_A} & \frac{\partial^2 J}{\partial F_R^2} & \frac{\partial^2 J}{\partial F_R\,\partial ER_A} & \frac{\partial^2 J}{\partial F_R\,\partial ER_R} \\ \frac{\partial^2 J}{\partial ER_A\,\partial F_A} & \frac{\partial^2 J}{\partial ER_A\,\partial F_R} & \frac{\partial^2 J}{\partial ER_A^2} & \frac{\partial^2 J}{\partial ER_A\,\partial ER_R} \\ \frac{\partial^2 J}{\partial ER_R\,\partial F_A} & \frac{\partial^2 J}{\partial ER_R\,\partial F_R} & \frac{\partial^2 J}{\partial ER_R\,\partial ER_A} & \frac{\partial^2 J}{\partial ER_R^2} \end{bmatrix}^{-1}} \quad (9)$$

By assuming no correlations among the variables, only the diagonal elements of the Hessian were used in *a posteriori* uncertainties calculation.

We evaluated the *a posteriori* uncertainties on partitioned photosynthetic fluxes on a typical day during summer (4 July 2012)

340 with assigned *a priori* uncertainties. The *a priori* uncertainty of gross assimilation ($\sigma_{F_A^b}$) was set to 10 µmol m^{-2} s^{-1} and of ecosystem respiration ($\sigma_{F_R^b}$) to 5 µmol m^{-2} s^{-1}, following Ogee et al. (2004) assuming less constraint on *a posteriori* results (Table 2). The uncertainty of the net CO_2 fluxes ($\sigma_{F_{CO_2}}$) was derived from Mann and Lenschow's model (Lenschow et al., 1994) and calculated for our site to be 2.5 µmol m^{-2} s^{-1} (Braden-Behrens et al., 2019). We also examined if σ_{F_A} could be reduced if more accurate net CO_2 fluxes were measured ($\sigma_{F_{CO_2}}$ = 0.5 µmol m^{-2} s^{-1}).

345 The uncertainty of measured ecosystem O_2 fluxes ($\sigma_{F_{O_2}}$) is unknown to us. Consequently, we used the results from the flux-gradient method evaluation (section 2.4.). In order to clearly quantify the effect of $\sigma_{F_{O_2}}$ and σ_{ER_A} on flux partitioning precision, we defined a $\sigma_{F_{O_2}}$ series ranging from 0.1 to 15 µmol m^{-2} s^{-1}, representing 90% quantile of random Δo measurement uncertainty (see section 2.4.), and a series of $\sigma_{ER_A^b}$ ranging from 0.001 to 0.1 mol mol^{-1}. $\sigma_{ER_R^b}$ was fixed to either 0.05 or 0.001 mol mol^{-1}.

350 Moreover, we assessed the impact of the model parameters ER_A, ER_{stem} and ER_{soil} by changing each by ±10% on the source partitioning results by estimating the absolute change in the *a posteriori* σ_{F_A}.

Table 2. Assigned *a priori* values and uncertainties to build the cost function, J, for the uncertainty estimation of using O_2 fluxes to partition net CO_2 fluxes.

variables	*a priori* values	*a priori* uncertainties
F_A	-15 µmol m^{-2} s^{-1}	10 µmol m^{-2} s^{-1}
F_R	5 µmol m^{-2} s^{-1}	5 µmol m^{-2} s^{-1}
ER_A	1.00 mol mol^{-1}	0.001 - 0.10 mol mol^{-1}
ER_R	1.10 mol mol^{-1}	0.05 or 0.001 mol mol^{-1}
F_{CO_2}	eddy covariance observations	2.5 or 0.1 µmol m^{-2} s^{-1}
F_{O_2}	CANVEG outputs	0.1 - 15 µmol m^{-2} s^{-1}

355 **3 Results**

3.1 Model performance

The model generally showed similar performance for F_{CO_2}, H and LE during both calibration and validation (Fig. 2), indicating robust model behavior as a multi-layer canopy flux simulator. The model validation for F_{CO_2} (R^2 = 0.82, slope = 1.016) was

generally better than for H ($R^2 = 0.7$, slope $= 0.879$) and LE ($R^2 = 0.77$, slope $= 1.02$) (Fig. 2b, 2d and 2f). The disagreement

360   between modeled and measured F_{CO_2} indicated some uncertainties in the parameters for soil and stem respiration as well as phenology in the model equations. The similar scale but opposite sign of y-intercepts for H and LE calibration simulations (Fig. 2c and 2e) indicated underestimation in H and the same amount of overestimation in LE. The slopes deviating from one for H and LE could come from a non-closure of the energy balance in the eddy covariance observations.

Due to potential variations in the ER model parameters (which were here taken from literature), we conducted a sensitivity

365   analysis to show how these parameters affected the modeled F_{O_2}. If ER_A was increased or decreased by 10%, the modeled F_{O_2} sum of the entire study period increased or decreased on average by 20.3% correspondingly. Similarly, a change by plus or minus 10% increments on ER_{soil} and ER_{stem} caused the F_{O_2} sum to decrease or increase by 8.6% and 1.7%, respectively. These results directly followed Eq. (1) where the derivative with respect to a specific ER gives the corresponding flux in percent. Oxygen fluxes were hence most sensitive to the ER of the largest carbon fluxes.

370
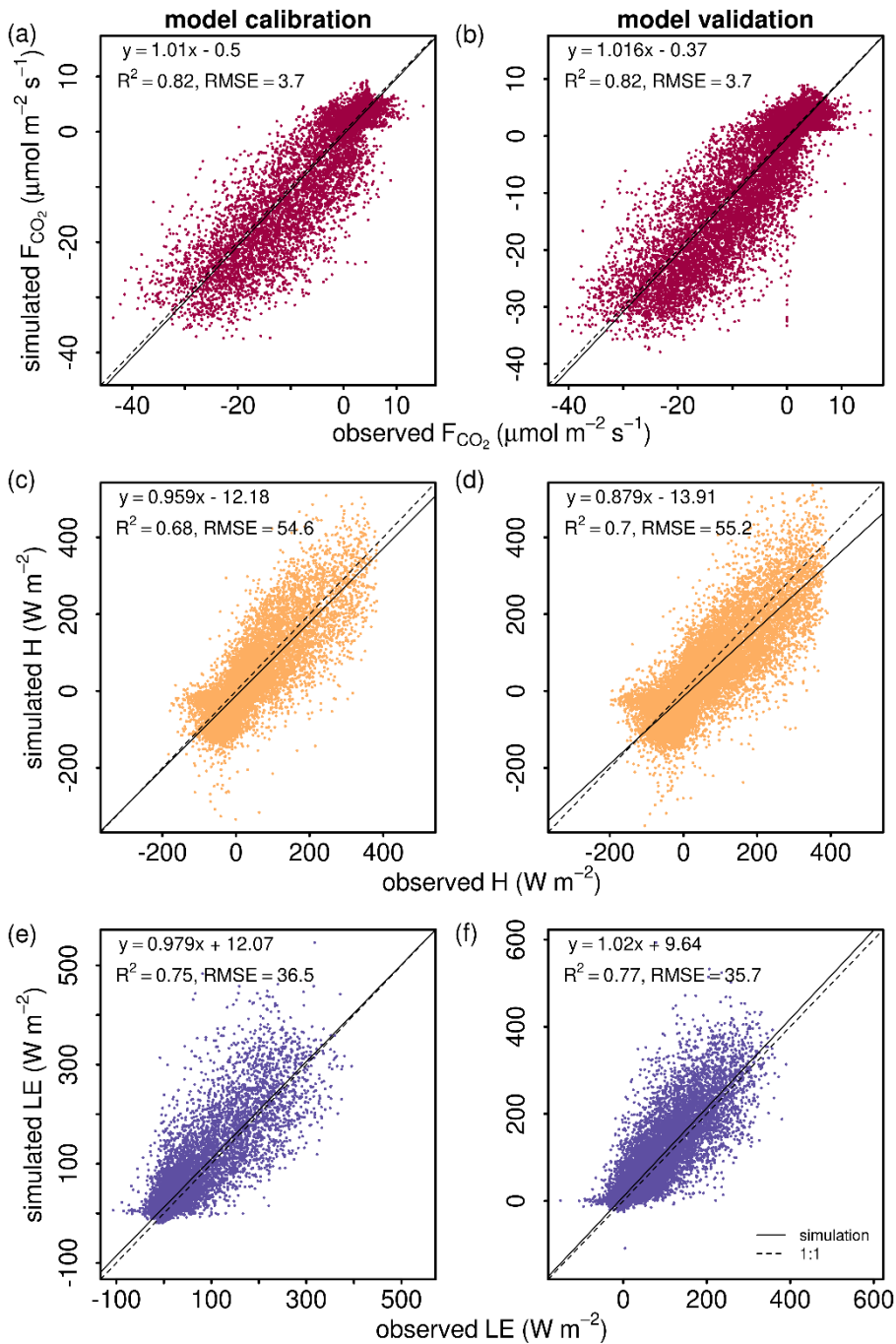
Figure 2. Comparison of (a), (b) net ecosystem CO_2 flux (F_{CO_2}), (c), (d) sensible (H), and (e), (f) latent (LE) heat flux from 2012 to 2016 between model simulations (y-axes) and eddy covariance observations (x-axes). The left column shows all hourly data points for the calibration period (2012-2013), and the right column shows all hourly data points for the validation period (2014-2016). The linear regression line function, coefficient of determination (R^2), and the root mean squared error (RMSE) are included in each panel. The dashed lines are the 1:1 lines.

3.2 Temporal dynamics of O_2:CO_2 exchange ratios

The median of the hourly ecosystem O_2:CO_2 exchange ratio (ER_{eco}) throughout the simulation period (2012-2016) was 1.08 mol mol^{-1}, where the annual medians did not differ between years. The annual mean ER_{eco} ranged from 1.06 to 1.12 mol mol^{-1} across the five years. Hourly ER_{eco} also varied seasonally and within the diel course, as shown as an example for the year 2012 in Figure 3a. During the non-growing season, ER_{eco} were constrained between 1.04 and 1.10 mol mol^{-1}, representing a mixture of the prevailing stem and soil respiration processes. During the growing season, ER_{eco} was close to 1.00 mol mol^{-1} during daylight hours, due to the dominance of photosynthetic processes, and sometimes even smaller than 1.00 mol mol^{-1}, when daytime F_{O_2} was smaller than daytime F_{CO_2}. This could occur with $ER_A = 1.00$ mol mol^{-1}, and ER_{stem}, ER_{soil} and $ER_{rd} >$ 1.00 mol mol^{-1} (following Eq. (1)) when more O_2 was consumed than CO_2 released for the respiratory fluxes, and thus the magnitude of net F_{O_2} was decreased. During nighttime in the growing season, ER_{eco} was > 1.00 mol mol^{-1}, representing a mixture of stem, soil and leaf dark respiration. For transition periods (sunrise and sunset), with flux magnitudes close to zero, ER_{eco} values were very high, owing to very small F_{CO_2}. Because ER_{eco} is a ratio, values could get extremely large and approach infinity as F_{CO_2} approached zero. However, since corresponding F_{O_2} values were also very low, these ER_{eco} values had very little effect on median and mean ER_{eco} of the overall ecosystem over a longer time period.

Within the sensitivity analysis, the initial annual median ER_{eco} of 1.08 mol mol^{-1} changed only by up to 0.02 mol mol^{-1} due to the change in ER_A or ER_{stem} by ±10%. Increasing or decreasing ER_{soil} had the largest impact, where median ER_{eco} increased or decreased to 1.00 or 1.17 mol mol^{-1}, respectively. Also here, the interannual difference between years was very small. A similar pattern could be found for the annual mean ER_{eco}, which varied between 1.04 and 1.15 mol mol^{-1} depending on ER_A and ER_{stem}, and varied even between 1.00 and 1.24 mol mol^{-1} due to ER_{soil}.

The median and mean of hourly O_2:CO_2 net assimilation ratio (ER_{An}) were 0.99 mol mol^{-1} and 0.97 mol mol^{-1}, respectively, for all growing seasons during the simulation period, and did not vary between years. In the sensitivity analysis, ER_{An} was only slightly impacted by changes in the model parameter of ER_A (ER_{stem} and ER_{soil} had no impact). Again, the seasonal and diel variations of ER_{An} in the year 2012 of the original simulation are shown in Figure 3b as an example. During nighttime, ER_{An} was equivalent to ER_{rd} and thus also dependent on T_{leaf} (Fig. 1b). With low T_{leaf} at the beginning or end of the growing season, ER_{An} was often smaller than 0.90 mol mol^{-1}. During daytime, when the magnitude of F_A was usually much larger than the magnitude of the opposing flux F_{rd}, ER_{An} was negatively correlated to T_{leaf}. Note that F_{rd} and ER_{rd} responded differently to T_{leaf}, that was, F_{rd} was a fraction of V_{cmax}, which had an optimal temperature at 27 °C (Table 1) while ER_{rd} was positively correlated with T_{leaf} (Fig. 1b). Consequently, during periods with high T_{leaf} and low irradiation, F_{rd} was small, but ER_{rd} was large and the magnitude of the O_2 flux of leaf respiration was larger than the magnitude of the CO_2 flux with $|-F_{rd} \cdot ER_{rd}| >$ $|F_{rd}|$. Moreover, $|-F_A \cdot ER_A|$ and $|F_A|$ were small with $ER_A = 1.00$ mol mol^{-1}. It followed that under these conditions and given model implementation, ER_{An} described the ratio of O_2 uptake and CO_2 uptake (both fluxes with the same sign), when more O_2

was consumed due to dark leaf respiration than released by assimilation ($|-F_{rd} \cdot ER_{rd}| > |-F_A \cdot ER_A|$). In addition, because values of F_A were below zero and values of F_{rd} were greater than zero, values of ER_{An} (Eq. (3)) laid mostly not between ER_A and ER_{rd}. Similar to ER_{eco}, high variations in ER_{An} were usually found during transition periods with low flux magnitudes.
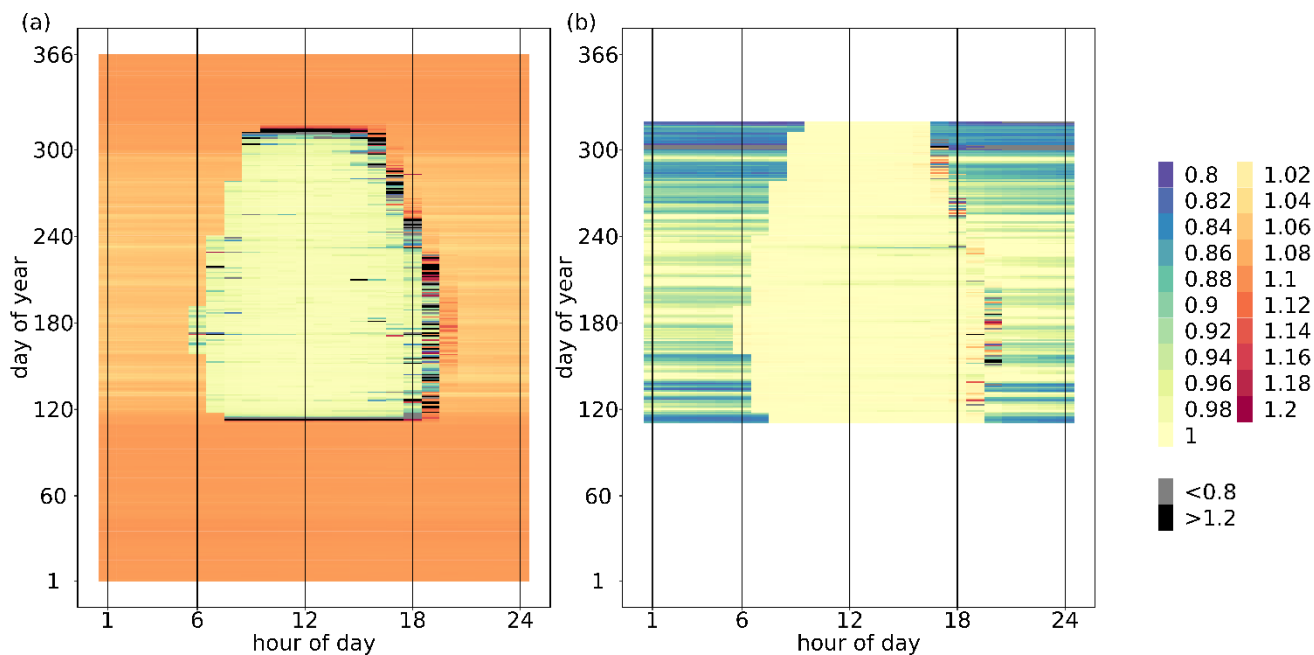
Figure 3. Temporal variations of (a) the exchange ratio of net ecosystem fluxes (ER_{eco}, mol mol^{-1}) and (b) the exchange ratio of net assimilation (ER_{An}, mol mol^{-1}) by hour of day and day of year in 2012. The exchange ratios were calculated as the ratio of the hourly F_{O_2} and F_{CO_2} (including storage terms) summed up over the entire canopy height. As a guide, 1st July is day 183.

3.3 Vertical profiles of O_2:CO_2 flux- and mole fraction-ratios

The vertical profiles of ER_{eco} and ER_{conc} differed temporally and spatially. Figure 4 shows the diel vertical profiles of ER^z_{eco} and ER^z_{conc} averaged over all growing seasons from 2012-2016 (between leaf$_{out}$ and leaf$_{fall\_complete}$). The mean diel ER^z_{eco} ranged from 0.985 to 1.10 mol mol^{-1} (Fig. 4a). ER^z_{eco} at the ground and bottom layers (z/ht ≤ 0.35) showed very little variability across the day reflecting the dominance of stem and soil respiration with fixed values of ER_{soil} and ER_{stem} (Fig. 4a). The upper levels of the canopy showed ER^z_{eco} between 0.99 and 1.04 mol mol^{-1} during the daylight period (6:00 to 20:00) due to the dominating fluxes of assimilation and stem respiration. The leaf dark respiration did not have a large impact on averaged daytime ER^z_{eco}. Moreover, the defined LAI and WAI distributions (Fig. 1a) were represented in the vertical profile of ER^z_{eco}, whereas the top canopy contained a larger proportion of sunlit leaves (z/ht > 0.75) than the middle part (0.35 < z/ht < 0.75). Hence, ER^z_{eco} in the top canopy was influenced more by fluxes of assimilation in daytime hours and was close to 1.00 mol mol^{-1}. Between z/ht = 0.3 and z/ht = 0.5, ER^z_{eco} was larger than 1.06 mol mol^{-1} during daytime due to higher respiratory processes than assimilation

affected by low radiation and relatively high temperatures. The ER^z_{eco} during nighttime (approximately before 6:00 and after 20:00) of the upper and middle canopy was usually larger than 1.04 mol mol^{-1} due to respiratory fluxes.

The mean diel ER^z_{conc} showed relatively small variations ranging from 1.115 to 1.15 mol mol^{-1} (Fig. 4b), and thus, closely matched the prescribed atmospheric O_2:CO_2 mole fraction slope of 1.15 (Table 1). Especially during nighttime (before 6:00 and after 20:00), ER^z_{conc} was mainly driven by the atmospheric O_2 and CO_2 background levels. However, bottom layers showed slightly lower values of ER^z_{conc}, down to 1.12 mol mol^{-1}, owing to an accumulation of CO_2 close to the soil surface produced by soil respiration and low turbulence. During daytime, the canopy air column was well mixed due to stronger turbulence. Nevertheless, ER^z_{conc} values were slightly lower in the top canopy layers towards late afternoon and sunset, caused by prevailing canopy respiration.
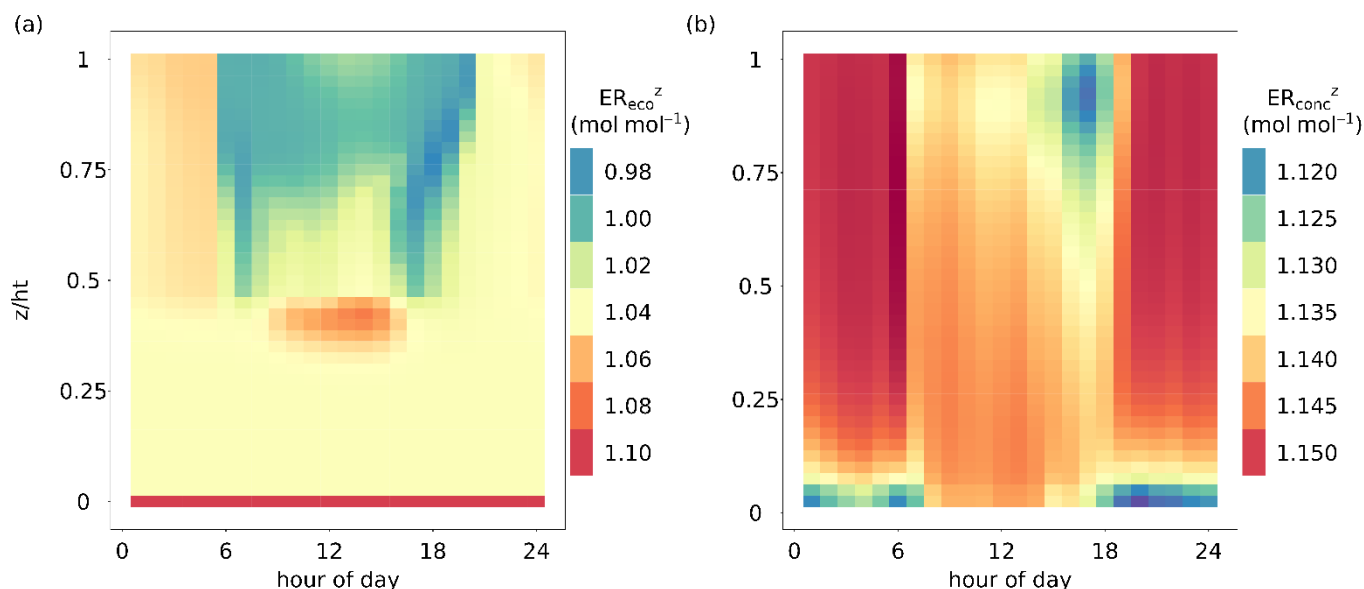
Figure 4. Comparison of the diel dynamics of the height dependent O_2:CO_2 flux- and mole fraction-ratios averaged over all growing seasons (day of year 110 to 320) from 2012 to 2016. (a) Vertical profile of the O_2:CO_2 flux-ratio inside the canopy (ER^z_{eco}, mol mol^{-1}), including the whole canopy domain and the soil component (z/ht = 0); (b) Vertical profile of the O_2:CO_2 mole fraction-ratio inside the canopy (ER^z_{conc}, mol mol^{-1}), including the whole canopy domain. The exchange ratios for specific canopy heights were derived as the slope of linear regressions fitted to O_2 and CO_2 fluxes or dry air mole fractions of multiple simulated time steps for each canopy layer.

3.4 Evaluation of the flux-gradient method to obtain O_2 fluxes

The vertical profiles of air temperature, water vapor, CO_2, and O_2 mole fractions were modeled for the entire CANVEG domain including 40 canopy layers and 80 atmosphere layers above the canopy. Figure 5 shows examples of vertical profiles for 12:00 p.m. to 13:00 p.m. (daytime) and 23:00 p.m. to 00:00 a.m. (nighttime) on 4 July 2012, an arbitrarily chosen sunny day.

Generally, during daytime the vertical profiles within the canopy (Fig. 5a and 5c) were mostly induced by radiative transfer, leaf photosynthesis, transpiration and autotrophic respiration, which were influenced by the vertical LAI and WAI distributions (Fig. 1a). Furthermore, soil evaporation and respiration resulted in higher water vapor and CO_2 mole fractions close to the soil surface. For the layers above the canopy (z/ht >1), the profiles changed monotonically. Daytime O_2 and CO_2 profiles (Fig. 5c)

455   showed a mirrored shape because the O_2 and CO_2 fluxes were contributing inversely to the atmospheric mole fractions. Nighttime water vapor and CO_2 profiles (Fig. 5d and 5d) showed a continuous decrease with height and the O_2 profile a continuous increase, due to the dominance of soil evaporation and soil, stem and leaf respiration in the lower layers being a sink for O_2. During nighttime, air temperature (Fig. 5b) was slightly lower at the canopy top than inside the canopy due to higher energy loss by emission of longwave radiation.

460   Based on these modeled vertical profiles and the corresponding flux (F_{CO_2}, H or LE, respectively), O_2 fluxes were calculated with the flux-gradient method and compared to the modeled O_2 fluxes from CANVEG, both corrected for the storage term. So in the following we always describe the ecosystem fluxes (turbulent fluxes plus storage terms). Figures 5e and 5f show the difference between the various flux-gradient methods derived and modeled F_{O_2} ($\Delta F_{O_2,(c,T,v)}$, (Eq. (7)) for the respective simulation hours, when the scalar gradients were derived from two heights (section 2.4). An F_{O_2} estimate and a $\Delta F_{O_2,(c,T,v)}$

465   value were obtained for each layer. Generally, ΔF_{O_2} derived with the flux-gradient method based on the CO_2 profile ($\Delta F_{O_2,c}$) was lower than ΔF_{O_2} derived from the temperature and water vapor profile ($\Delta F_{O_2,T}$, $\Delta F_{O_2,v}$; Fig. 5e and 5f). For daytime conditions (Fig. 5e), the mean $\Delta F_{O_2,c}$, $\Delta F_{O_2,T}$ and $\Delta F_{O_2,v}$ above the canopy were 0.030 ± 0.09 µmol m^{-2} s^{-1}, 1.55 ± 0.54 µmol m^{-2} s^{-1} and -4.26 ± 0.63 µmol m^{-2} s^{-1}, respectively (Table 3). There was little vertical variation in $\Delta F_{O_2,(c,T,v)}$ above the canopy for nighttime (Fig. 5f). Here, the mean $\Delta F_{O_2,c}$, $\Delta F_{O_2,T}$ and $\Delta F_{O_2,v}$ were -0.53 ± 0.04, -1.98 ± 0.20 and -0.47 ± 0.24 µmol m^{-2} s^{-1}

470   , respectively. By applying the three-heights flux-gradient method after Faassen et al. (2022), ΔF_{O_2} for the daytime hour had a similar magnitude for $\Delta F_{O_2,c}$ with -0.13 µmol m^{-2} s^{-1} and for $\Delta F_{O_2,v}$ with -4.31 µmol m^{-2} s^{-1}, and was larger for $\Delta F_{O_2,T}$ with 4.72 µmol m^{-2} s^{-1}. The corresponding nighttime $\Delta F_{O_2,c}$, $\Delta F_{O_2,T}$ and $\Delta F_{O_2,v}$ derived from the three-heights flux-gradient method were -0.50, -2.41 and -0.66 µmol m^{-2} s^{-1}, indicating the similar $\Delta F_{O_2,c}$ and $\Delta F_{O_2,v}$, but a larger magnitude of $\Delta F_{O_2,T}$ than with two-heights flux-gradient method.

475

Table 3. Difference between the F_{O_2} estimations derived by the flux-gradient method ($\tilde{F}_{O_2,(c,T,v)}$, based on $\tilde{F}_{CO_2}$, $\tilde{H}$ or $\tilde{LE}$ and their respective vertical scalar profile) and by model simulations ($\tilde{F}_{O_2,CANVEG}$) for above canopy fluxes and for day- and nighttime individually. Results of the two-height approach are shown as the mean and standard deviation of flux-gradients derived between z/ht = 2 and each layer below above the canopy. Also results of the three-height approach are shown, where the flux-gradient was

480   derived between three fixed heights (z/ht = 1.05, 1.45 and 2 with ht = 37.5 m).

variables	two heights		three heights	
(µmol m^{-2} s^{-1})	daytime	nighttime	daytime	nighttime
$\Delta F_{O_2,c}$	0.030 ± 0.09	-0.53 ± 0.04	-0.13	-0.50

$\Delta F_{O_2,T}$	1.55 ± 0.54	-1.98 ± 0.20	-4.31	-2.41
$\Delta F_{O_2,v}$	-4.26 ± 0.63	-0.47 ± 0.24	4.72	-0.66

The $\Delta F_{O_2,(c,T,v)}$ within the canopy during daytime increased and was highly variable for all three methods due to the presence of sources and sinks, and non-linearity of the gradients (Fig. 5e). $\Delta F_{O_2,c}$ and $\Delta F_{O_2,T}$ showed hyperbolic shapes with very low (< -50 µmol m^{-2} s^{-1}) and high values (> 50 µmol m^{-2} s^{-1}) where the CO_2 dry air mole fractions or the temperatures, respectively, were very close to the conditions at the top measurement height, and so the gradients were very small. The sudden jumps from large positive to large negative values were caused by the change in signs of Δc and ΔT.

To guarantee a large gradient, the heights with z/ht = 2 and z/ht = 1.05 were used in inferring F_{O_2} from vertical CO_2, temperature and water vapor gradients for the following analysis. Figures 6a, 6b, and 6c show the median diel courses of $\Delta F_{O_2,c}$, $\Delta F_{O_2,T}$ and $\Delta F_{O_2,v}$ for all growing seasons from 2012-2016. Assuming that with these heights the gradients were large enough, the inferred F_{O_2} agreed well with modeled F_{O_2} for $\Delta F_{O_2,c}$ throughout the median diel course ranging from -0.45 to -0.15 µmol m^{-2} s^{-1} (Fig. 6a). The medians of $\Delta F_{O_2,T}$ and $\Delta F_{O_2,v}$ indicated that $F_{O_2,T}$ was overestimated by up to 1.59 µmol m^{-2} s^{-1} and $F_{O_2,v}$ underestimated by up to 5.43 µmol m^{-2} s^{-1} during daytime hours (Fig. 6b and 6c). The standard deviations of $\Delta F_{O_2,(c,T,v)}$ reflected the diel variation of turbulent conditions and vertical gradients, which were also dependent on the eddy diffusivity. The nighttime standard deviation of $\Delta F_{O_2,v}$ was relatively large, but smaller for $\Delta F_{O_2,T}$. The latter produced more outliers during daytime, especially during times of sunrise and sunset. The standard deviation of $\Delta F_{O_2,c}$ was relatively low and usually < 10 µmol m^{-2} s^{-1} across all times of the day except at 08:00, 12:00 and 19:00 o'clock (Fig. 6a).

The above analysis evaluated the flux-gradient method solely regarding the characteristics and dynamics of various scalar gradients. Moreover, accurate and precise measurements of the scalars are also necessary for a satisfactory performance of this method. We added a random uncertainty to our modeled O_2 mole fractions to simulate gradient measurements with the current instrument uncertainty (Δo in Eq. (6)). Figure 6d shows the distribution of the differences ($\sigma_{F_{O_2}}$) between the F_{O_2} estimates based on the flux-gradient method including a random measurement uncertainty in Δo or not. For this analysis, only hourly timesteps within all growing seasons from 2012-2016 were chosen with $\Delta o \geq 1$ ppm, when O_2 mole fractions increased with decreasing height above the canopy due to prevailing gross assimilation over respirations during daytime. The median of resulting $\sigma_{F_{O_2}}$ was 0.20 µmol m^{-2} s^{-1} and thus very close to zero. Here, we extracted the 10% and 90% quantile of $\sigma_{F_{O_2}}$ = -14.2 and 14.5 µmol m^{-2} s^{-1}. Thus, we used 15 µmol m^{-2} s^{-1} as the upper limit of $\sigma_{F_{O_2}}$ in the evaluation of the flux partitioning approach (section 3.5).
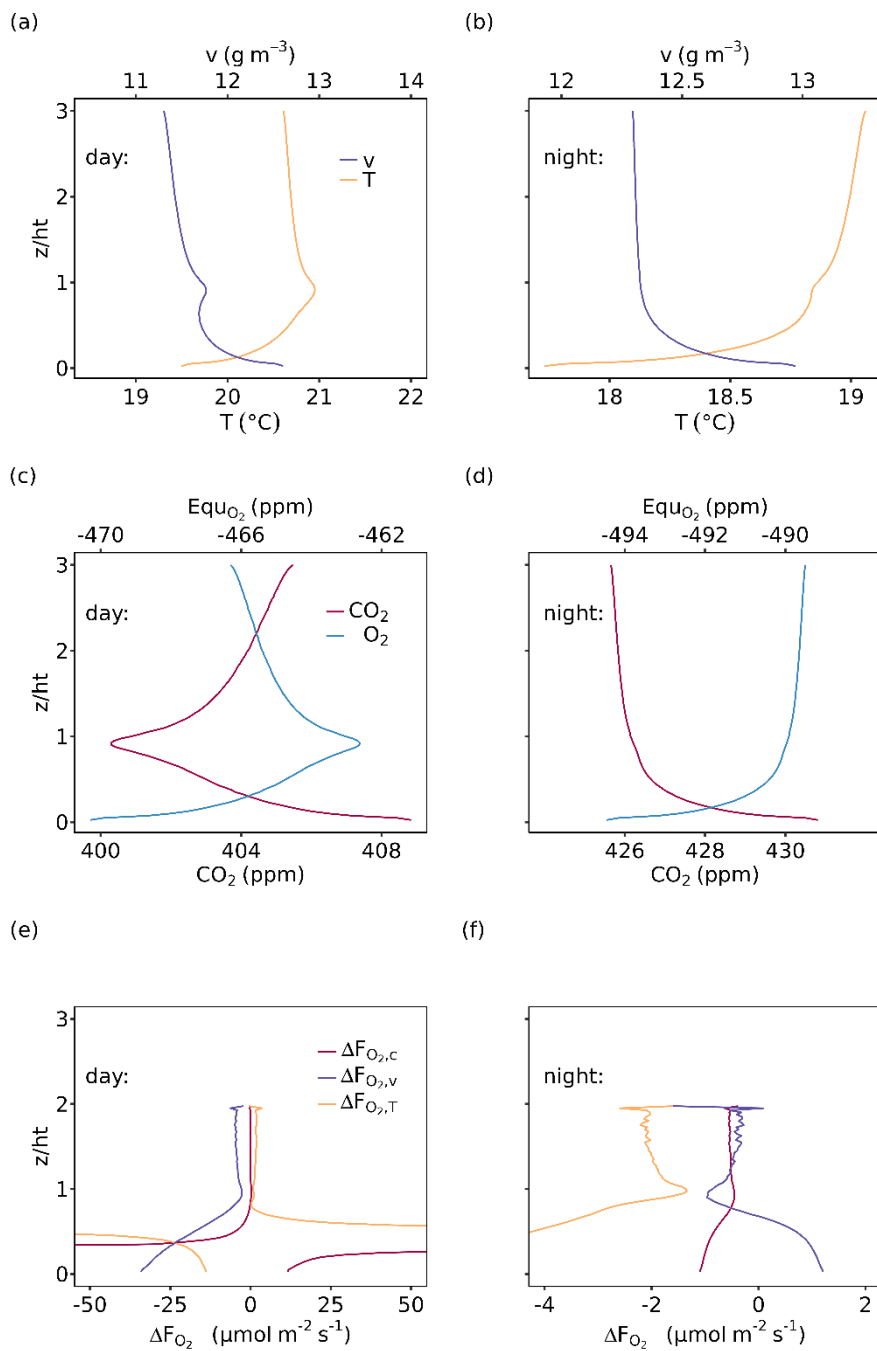
Figure 5. Vertical profiles of (a), (b) air temperature (T) and water vapor (v), and (c), (d) CO_2 and O_2 mole fractions of the entire model domain, where O_2 mole fractions are shown as the difference from 209750 ppm (Equ_{O_2}, 209750 ppm was derived as the intercept of the relationship between measured atmospheric O_2 and CO_2 mole fractions, cf. Table 1). (e), (f) $\Delta F_{O_2,(c,T,v)}$ that resulted from Eq. (7) (section 2.4). The left panels (a), (c) and (e) show mean profiles for 12:00 p.m. to 13:00 p.m. (daytime) and the right panels (c), (d) and (f) for 23:00 p.m. to 00:00 a.m. (nighttime), all for 4 July 2012. The flux-gradient method was applied for the

gradients between a top measurement height at z/ht = 2 and each layer below, and based on profiles and fluxes of CO_2, H and LE ($\Delta F_{O_2,c}$, $\Delta F_{O_2,T}$ and $\Delta F_{O_2,v}$).
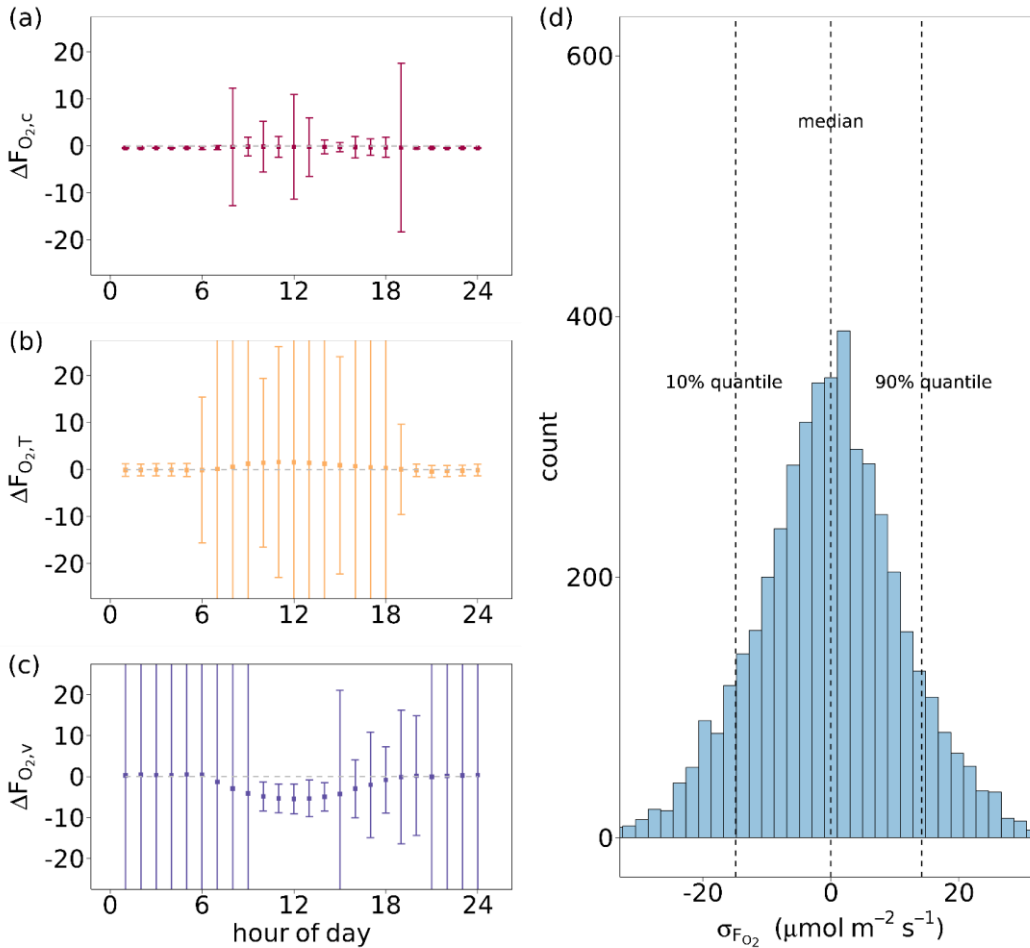
Figure 6. (a), (b), (c) Median diel cycles of the differences between O_2 fluxes derived by flux-gradient method and by CANVEG simulation ($\Delta F_{O_2,(c,T,v)}$) for all growing seasons from 2012-2016. The flux-gradient method was applied for the gradients between z/ht = 2 and z/ht = 1.05, and based on profiles and fluxes of (a) CO_2, (b) H and (c) LE ($\Delta F_{O_2,c}$, $\Delta F_{O_2,T}$ and $\Delta F_{O_2,v}$). The error bars indicate the standard deviation of $\Delta F_{O_2,(c,T,v)}$ by hour. (d) Histogram of uncertainties in F_{O_2} ($\sigma_{F_{O_2}}$) derived by the flux-gradient method based on CO_2 profile and fluxes, when a random uncertainty in O_2 mole fractions (Δo) was included. The uncertainty in Δo followed a normal distribution with mean = 0 and a standard deviation of 0.7 ppm (Pickers et al., 2017). In order to include daytime hours with an active canopy for the estimation of $\sigma_{F_{O_2}}$, $\Delta o \geq 1$ ppm was used as a filter, assuming higher oxygen dry air mole fractions close to the canopy than in the top domain layers.

3.5 Uncertainties in partitioning net ecosystem CO₂ fluxes based on O₂ fluxes

For the test day from 07:00 to 19:00 on 4 July 2012, model output of hourly F_{O_2} was used to derive the main CO_2 flux components. The *a posteriori* uncertainties on the partitioned fluxes of gross assimilation (σ_{F_A}) decreased significantly with decreasing uncertainties of σ_{ER_A} and $\sigma_{F_{O_2}}$, indicating the importance of reducing errors in ER and O₂ flux measurements (Fig. 7). The *a priori* uncertainties had strong effects on *a posteriori* uncertainties, because a large $\sigma_{F_A^b}$ allowed large $| F_A - F_A^b |$ to reach a minimum J value and vice versa (Eq. (8)). Without the constraints of *a priori* uncertainties (Fig. 7a), σ_{F_A} reached 193 µmol m⁻² s⁻¹ at its maximum, then reduced with smaller $\sigma_{F_{O_2}}$ and σ_{ER_A} to 28 µmol m⁻² s⁻¹, which was still larger than the *a priori* value (Table 2). If *a priori* uncertainties ($\sigma_{F_A^b}$, $\sigma_{F_R^b}$, $\sigma_{ER_A^b}$, $\sigma_{ER_R^b}$) were included (Fig. 7b and 7c), σ_{F_A} was much lower. When assuming an uncertainty for the net CO₂ fluxes ($\sigma_{F_{CO_2}}$) of 2.5 µmol m⁻² s⁻¹, σ_{F_A} showed very little variation and ranged between 4.74 and 4.88 µmol m⁻² s⁻¹ remaining close to the minimum of the chosen *a priori* uncertainty in F_A and F_R (Fig. 7b). When assuming more accurate F_{CO_2} and ER_R measurements with $\sigma_{F_{CO_2}}$ = 0.5 µmol m⁻² s⁻¹ and σ_{ER_R}= 0.001 mol mol⁻¹, σ_{F_A} was reduced to a minimum of 1.43 µmol m⁻² s⁻¹ (Fig. 7c). A moderate level of *a priori* uncertainties in O₂ fluxes and ER_A (bold black lines in Fig. 7c) resulted in σ_{F_A} = 4.48 µmol m⁻² s⁻¹ for our test day. In this case, the partitioned F_A was 28.3 µmol m⁻² s⁻¹, which was about 6% lower than the estimated gross assimilation obtained with the eddy covariance technique (F_A^b = 30.2 µmol m⁻² s⁻¹). In regard to the sensitivity analysis, σ_{F_A} was only slightly impacted by ER_A. σ_{F_A} ranged from 1.42 to 4.83 µmol m⁻² s⁻¹ for the case of the lower *a priori* uncertainty (with $\sigma_{F_{CO_2}}$ = 0.5 µmol m⁻² s⁻¹ and σ_{ER_R}= 0.001 mol mol⁻¹).
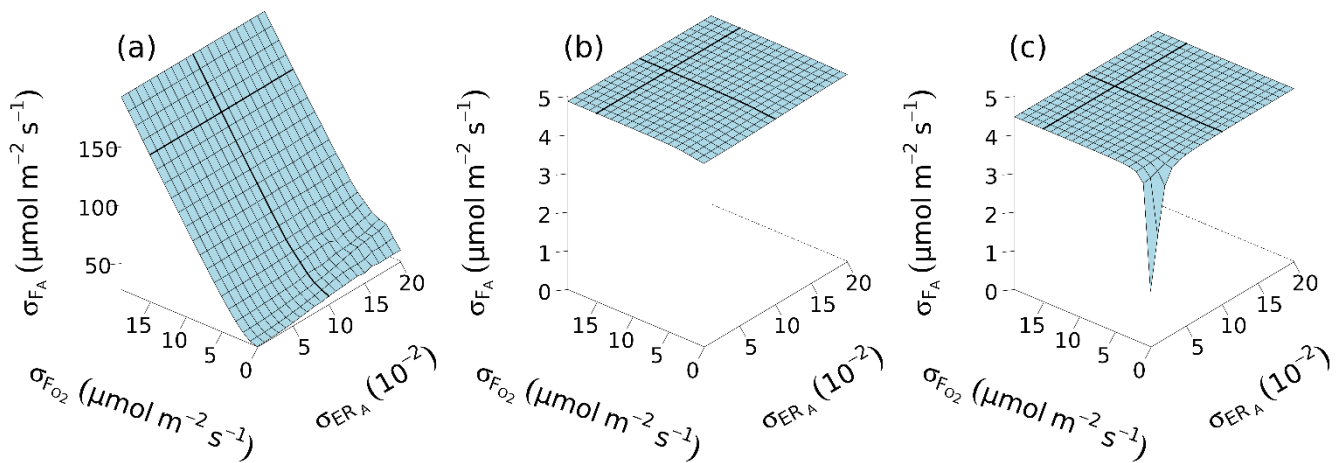
545 **Figure 7. Uncertainty in partitioned gross assimilation CO_2 flux (F_A) determined from eddy covariance net ecosystem CO_2 flux (F_{CO_2}) with net ecosystem O_2 flux (F_{O_2}), O_2:CO_2 ratio of gross assimilation (ER_A) and ecosystem respiration (ER_R) on 4 July 2012; (a) Optimized *a posteriori* uncertainty of F_A (σ_{F_A}) without *a priori* F_A values and uncertainties; (b) Optimized σ_{F_A} including all of the *a priori* terms in the J function as written in Eq. (8), with *a priori* uncertainty of F_{CO_2} ($\sigma_{F_{CO_2}}$) = 2.5 µmol m^{-2} s^{-1} and *a priori* uncertainty of ER_R ($\sigma_{ER_R^b}$) = 0.05 mol mol^{-1}; (c) Same cost function as for (b) but with $\sigma_{F_{CO_2}}$ = 0.5 µmol m^{-2} s^{-1} and $\sigma_{ER_R^b}$ = 0.001 mol mol^{-1}. The**
550 **bold black lines show the practical optimization test with $\sigma_{ER_A^b}$ and $\sigma_{F_{O_2}}$ around 0.01 mol mol^{-1} and 15 µmol m^{-2} s^{-1}, respectively (cf. Figure 6d).**

4 Discussions

4.1 Model set-up and model performance

555 We added O_2:CO_2 exchange ratios and O_2 flux processes into the one-dimensional, multi-layer atmosphere-biosphere gas exchange model, CANVEG. To represent natural atmosphere-ecosystem exchange satisfactorily, we first calibrated and validated the model based on eddy covariance CO_2 and energy flux observations from a temperate deciduous forest in Leinefelde, Germany, from 2012-2016. In a previous study, model performance was evaluated based on hourly CO_2, water vapor and energy fluxes in temperate oak forests (Baldocchi and Wilson, 2001). That evaluation, for hourly F_{CO_2}, yielded a

560 slope = 1.09 of the regression between observations and simulation with an R^2 = 0.82, which is comparable to our results (slope = 1.02 and R^2 = 0.82, Fig. 2b). The model application in a deciduous temperate forest in central Germany (Knohl and Baldocchi, 2008) also showed a high match between hourly modeled and measured F_{CO_2} (slope = 0.997, R^2 = 0.857). In addition, Hanson et al. (2004) compared the CANVEG model with seven other stand-level models where CANVEG performed very well (slope = 0.93, R^2 = 0.82) based on simulated F_{CO_2}. In our study, the comparison between hourly LE simulation and

565 observations obtained a regressed slope = 1.02 and R^2 = 0.77 (Fig. 2f), indicating a better model performance than for daily evapotranspiration by Hanson et al. (2004) (slope = 1.17, R^2 = 0.73). Knohl and Baldocchi (2008) found a slope = 0.926 and R^2 = 0.825 for hourly LE simulation, and a slope = 1.021 and R^2 = 0.869 for hourly H simulation, indicating an underestimation of LE and a small overestimation of H. In our study, we observed an overestimation of LE and underestimation of H. The model performance (in regard to the slope, R^2 and RMSE) in the energy fluxes was generally lower than for CO_2 flux

570 simulations because fitted parameters mainly affected the CO_2 fluxes and leaf assimilation (Table 1). By adjusting the assimilation rate, only transpiration was also changed, which then had an impact on LE and H. The non-unity slope of H and LE could also point to the non-closure of the energy balance in the eddy covariance observations.

Furthermore, the modeling error could be caused by the implemented soil respiration algorithm, which did not consider the influence of soil water changes. Moreover, parameters for soil respiration were only calibrated based on eddy covariance

575 observations (F_{CO_2} and F_R) on ecosystem scale, where independent chamber measurements would be beneficial. Moreover, an error in the seasonality of carbon and energy fluxes could be introduced by the uncertainty in leaf growth phenology and annual LAI. Although we simulated fluxes from 2012 to 2016, the total leaf-full LAI and leaf growth phenology parameters (Table

1) were only measured in the year 2015 and kept constant across the modeling period (Table 1). Adjusting LAI annually would only affect the timing of the fluxes, but not the overall O_2:CO_2 exchange ratio (ER) pattern.

580   This study used fixed ER parameter values owing to the lack of direct chamber O_2 and CO_2 flux measurements for leaf, stem and soil flux components at our study site. The O_2:CO_2 exchange ratio of gross assimilation (ER_A) was set to 1.00 mol mol^{-1} (Table 1), describing the production of carbohydrates by gross assimilation. Busch et al. (2018) described how plants use nitrogen while assimilating CO_2, resulting in carbon loss from the photorespiratory pathway in the form of glycine and serine. Since nitrogen assimilation increases O_2 emissions but has smaller effects on CO_2 uptake, incorporating nitrogen assimilation

585 in the Farquhar et al. (1980) photosynthesis model would help to represent photosynthetic O_2 emissions more mechanistically in models. In this case, environmental conditions such as nitrogen fertilization and utilization would cause different ER_A values.

    Studies obtaining exchange ratios of O_2 and CO_2 via chamber measurements at the soil- or stem-scale often state the so-called apparent respiratory quotient (ARQ), which is defined as the ratio of CO_2 efflux to O_2 uptake (Angert et al., 2012; Helm et al., 2021; Hilman and Angert, 2016; Hilman et al., 2022). Thus, ARQ could be compared to our ER_{soil} or ER_{stem} by taking

590 the inverse of ARQ, which is the CO_2:O_2 conductance ratio, following Hilman and Angert (2016). However, ARQ is also influenced by biotic and abiotic non-respiratory processes such as dissolution and refixation of respired CO_2 in the xylem sap (Angert et al., 2012; Hilman and Angert, 2016; Hilman et al., 2022), so we expect differences between the various quantities. Furthermore, studies state the so-called oxidative ratio (OR) based on the elemental analysis of organic material. OR is based on the stoichiometry of the respiratory product or net synthesized biomass, which represents the oxidation state of respiratory

595 substances (Hilman et al., 2022; Juergensen et al., 2021).

    All ARQ values from the cited references were converted to ER_{stem} or ER_{soil} for easier comparison. The ER_{stem} parameter = 1.04 mol mol^{-1} used in this study was derived by Randerson et al. (2006) based on the OR of chemical compositions (lipid, lignin, protein, soluble phenolic etc.) assigned to woody stems. Hilman and Angert (2016) measured a mean ER_{stem} = 1.47 mol mol^{-1} (ARQ = 0.68 ± 0.04 mol mol^{-1}) with direct continuous measurements for an apple tree. In addition, ER_{stem} also showed

600 variations between 1.22 and 1.61 mol mol^{-1} (ARQ = 0.62 to 0.82 mol mol^{-1}) during the measurement period (Hilman and Angert, 2016). The ER_{stem} varied between 1.28 and 2.56 mol mol^{-1} (ARQ = 0.39 to 0.78 mol mol^{-1}) with the mean of 1.69 mol mol^{-1} (ARQ = 0.59 mol mol^{-1}) among tropical, temperate, and Mediterranean forests (Hilman et al., 2019). In addition, dry or wet environmental conditions lead to a seasonal variation in ER_{stem} (Angert et al., 2012).

    The global OR of soils is suggested to be equal 1.10 ± 0.05 (Severinghaus, 1995). According to Hockaday et al. (2015), the

605 soil OR is 1.006 at ambient CO_2 level and increases to 1.054 with elevated CO_2 level. Worrall et al. (2013) also derived a global soil OR = 1.04. Seibt et al. (2004) obtained an ER_{soil} = 0.94 mol mol^{-1} with field chamber measurements, while Ishidoya et al. (2013) obtained ER_{soil} = 1.11 mol mol^{-1}. ER_{soil} also showed seasonal variations from about 1.11 mol mol^{-1} (ARQ = 0.9 mol mol^{-1}) during late spring and summer to about 1.43 mol mol^{-1} (ARQ = 0.7 mol mol^{-1}) during winter in a Mediterranean mixed conifer forest (Hicks Pries et al., 2020). Depending on ecosystem type, such as alpine areas, temperate, Mediterranean

610 or tropical forests, and on sampling strategies, such as sampling of soil air or bulk soil, measured ER_{soil} varied between 0.88 to 4.35 mol mol^{-1} (ARQ = 0.23 to 1.14 mol mol^{-1}) (Angert et al., 2015; Angert et al., 2012; Hilman et al., 2022). These

variabilities related to seasons, forest types and ecosystem processes strongly suggest that site specific ER_{stem} and ER_{soil} should be used in O_2 flux simulations. A logarithmic relationship between soil ARQ and soil temperature, as found by Hilman et al. (2022), could also be introduced to future soil O_2 flux models. Due to this high variance between derived ER of these different

615 studies, we conducted a sensitivity analysis by changing ER_A, ER_{stem} or ER_{soil} by ±10% to show how these parameters affected the modeled F_{O_2}, ER_{eco} and ER_{An}. Furthermore, we assessed the impact of these model parameters on the source partitioning results. In summary, the model simulations showed a small sensitivity towards the model parameter settings. The modeled F_{O_2} sum was mostly sensitive to ER_A, which corresponded to the largest flux component. ER_{eco} and ER_{An} changed by less than 10% in each case. The uncertainty in the source partitioning results were mostly driven by the uncertainty of O_2 flux estimates

620 ($\sigma_{F_{O_2}}$) and much less by the ER parameters. Generally, all model simulations yielded the same tendency and pattern of exchange ratios.

4.2 Temporal and vertical dynamics of O_2:CO_2 exchange ratios

The O_2:CO_2 flux exchange ratio (ER_{eco}) quantifies the simultaneous canopy-atmosphere gas exchange of the whole ecosystem. We obtained ER_{eco} by aggregating simulated O_2 and CO_2 fluxes of all canopy layers and taking the ratio or by deriving the

625 slopes of linear regressions fitted to O_2 and CO_2 fluxes of multiple simulated time steps for each canopy layer (ER^z_{eco}). The temporal variations in ER_{eco} arose from diel and seasonal variations in the flux contributions of gross assimilation and respiration to net ecosystem O_2 and CO_2 exchange. Since assimilation and respiration are two individual processes, which are influenced by two differing main drivers - photosynthetic photon flux density and temperature - they usually show shifted diel cycles. Furthermore, fluxes from respiration consist of various components originating from various sources (e.g., respiration

630 by heterotrophs, leaves or roots), which can also differ in their diel cycles, in their ER and in their proportions of total O_2 and CO_2 ecosystem fluxes. Further studies should obtain ER independently with respective chamber measurements in order to separate environmental effects (e.g., radiation, temperature, humidity) on each componental O_2 and CO_2 fluxes.

The ER_{eco} contains information about the turbulent flux exchange, as well as the O_2 and CO_2 storage terms between soil surface and measurement height. Our study focused on the whole ecosystem O_2 and CO_2 exchange ratio including storage terms.

635 Annual mean ER_{eco} ranged from 1.06 to 1.12 mol mol^{-1} within the five years and estimates of ER^z_{eco} varied between 0.99 and 1.10 mol mol^{-1} with height in the canopy (Fig. 4a). Seibt et al. (2004) reported daytime net turbulent ER (considering turbulent fluxes and not including storage terms) between 1.26 and 1.38 mol mol^{-1}, which they derived with a one-box model. Next to the in- or exclusion of storage terms and the usage of different models, differences between Seibt et al. (2004)'s work and ours could also be caused by the difference in considered time periods: our simulations covered five years' growing seasons of O_2

640 and CO_2 fluxes between the canopy and the atmosphere, and Seibt et al. (2004) focused on July and August between 1999 and 2001. Moreover, we used different componental ER parameters (Table 1) in our simulations.

Diel ER_{An} variations reflected separate responses of gross assimilation and leaf dark respiration to temperature. The median and mean of hourly ER_{An} were 0.99 and 0.96 mol mol^{-1}, respectively, for all growing seasons during the study period. However,

ER_{An} showed extreme values during transition hours with low flux magnitudes (Fig. 3b). Ishidoya et al. (2013) found ER_{An}
values close to 1.02 mol mol^{-1} via leaf chamber measurements. According to Seibt et al. (2004), ER_{An} ranged between 1.04
and 1.20 mol mol^{-1} observed also via chamber measurements when flux rates were between 2 and 5 µmol m^{-2} s^{-1}. A lower flux
rate (1.7 µmol m^{-2} s^{-1}) lead to a higher variability in ER_{An} (Seibt et al., 2004). The divergence between our ER_{An} estimates
(which were close to 1.00 mol mol^{-1}) and to the chamber measurements could be caused by the utilization of varying nitrogen
sources that would increase ER_{An} (Seibt et al., 2004).

The mole-based O$_2$:CO$_2$ exchange ratio (ER_{conc}) is determined by the atmospheric background mole fractions of O$_2$ and CO$_2$,
by the distributions and dynamics of sources and sinks, and the turbulence inside the canopy. ER_{conc} is usually derived based
on the slopes of Deming regressions of observed O$_2$ and CO$_2$ mole fractions accounting for uncertainty in both variables (Battle
et al., 2019; Ishidoya et al., 2020). Our results of ER_{conc} and ER_{eco} confirmed that ER_{conc} cannot represent simultaneous O$_2$ and
CO$_2$ exchange as ER_{eco}, which was also recently found by Faassen et al. (2022). We also estimated ER^z_{conc} for each canopy
layer representing O$_2$ and CO$_2$ mole fractions of air on certain canopy heights. The mean diel ER^z_{conc} showed only very small
variations ranging from 1.12 to 1.15 mol mol^{-1} within the diel course. Battle et al. (2019) observed an average $ER_{conc} = 1.081$
± 0.007 mol mol^{-1} in a mixed deciduous forest over a six-years period and $ER_{conc} = 1.03 \pm 0.01$ mol mol^{-1} on two summer days
in July 2007. Their ER_{conc} measurements also showed temporal variations on a 6-hour basis between 0.85 and 1.15 mol mol^{-1}.
Seibt et al. (2004) measured and modelled ER_{conc} during day- and nighttime at several sites and obtained values varying
between 1.04 and 1.19 mol mol^{-1}. Ishidoya et al. (2013) observed daily average $ER_{conc} = 0.94 \pm 0.01$ mol mol^{-1}, with daytime
$ER_{conc} = 0.87 \pm 0.02$ mol mol^{-1} and nighttime $ER_{conc} = 1.03 \pm 0.02$ mol mol^{-1}. Ishidoya et al. (2013) also built a one-box canopy
O$_2$/CO$_2$ budget model applying the same parameter values $ER_A = 1.00$ mol mol^{-1} and $ER_R = 1.10$ mol mol^{-1} as our study. Their
observed daytime $ER_{conc} = 0.87$ mol mol^{-1} agrees with their modeled net turbulent $ER = 0.89$ mol mol^{-1}. Our modeled ER^z_{conc}
estimates showed a lower temporal variability within the mean diel course than in the cited studies. This is to a large part due
to background O$_2$ that was fixed to 1.15 of atmospheric CO$_2$ mole fractions (Table 2). One would expect, though, that this ratio
might be lower during summer and most probably has also a diel cycle. Future work could include continuous measurements
at the site resulting in a varying background value and potentially larger diel and seasonal variability. It is also possible that
mixing in CANVEG was too strong so that modeled ER^z_{conc} was excessively influenced by the background value. This could
be improved in future by comparing modelled temperature, water vapor and CO$_2$ mole fractions with measured mole fractions
in different canopy heights, which have become standard measurements at eddy covariance sites in forests now.

4.3 Estimation of ecosystem O$_2$ fluxes and applications

Eddy covariance measurements, as typically conducted for CO$_2$ fluxes, are currently not possible for O$_2$ fluxes, because no
sufficiently fast and precise O$_2$ analyzer is commercially available, yet (except for a self-made, non-commercial vacuum
ultraviolet (VUV) absorption analyzer developed by Stephens et al. (2003)). Requirements would be a precision of below 1
ppm against a background concentration of 210 000 ppm on a high, turbulence resolving measurement frequency (Keeling and
Manning, 2014). However, vertical profiles of air temperature, water vapor, CO$_2$ and O$_2$ mole fractions can already be obtained

with high precision. With our modeled vertical profiles, we determined O_2 fluxes based on the flux-gradient approach, testing various profile set-ups and the necessary instrument precision for O_2 mole fraction measurements (Fig. 5 and 6). By choosing various heights to derive the mole fraction gradients, we confirmed that the selected heights should both be above the canopy.

680 This guarantees that the profiles are differentiable as there are no sources or sinks between sampling heights, and that the eddy diffusivity of O_2 is the same as of the other corresponding scalars (Baldocchi et al., 1988). In addition, the mole fraction difference between the two heights should be as large as possible to decrease the uncertainty in O_2 flux estimates. Here, we selected amongst others heights at $z/ht = 1.05$ and $= 2$ to obtain large gradients. Faassen et al. (2022) applied the flux-gradient method to estimate O_2 fluxes in a boreal forest with a canopy height $= 18$ m. Their measurements were conducted between 23

685 m and 125 m for the vertical scalar gradient, reaching about seven times the canopy height. Such a large distance between measurement heights in a profile system is usually only feasible for cropland, grassland or peatland study sites with low vegetation. For high vegetation, such as forest sites, a tall tower is needed (as in Faassen et al., 2022). However, by choosing two measurement heights with a large distance (e.g., multiple tens of meters), the difference between the footprint extensions of each height becomes also large, potentially resulting in erroneous flux estimates. If, for instance, the vertical CO_2 gradient

690 could be doubled, the uncertainty in F_{O_2} fluxes caused by the measurement uncertainty of O_2 gradients would be reduced by 50% according to Eq. (6).

The median differences between F_{O_2} derived with the flux-gradient method and modeled F_{O_2} ($\Delta F_{O_2,(c,T,v)}$) were generally < 5.5 $\mu mol\ m^{-2}\ s^{-1}$, independent of which scalar concentrations and fluxes were used for the latter. However, $\Delta F_{O_2,v}$ and $\Delta F_{O_2,T}$ deviated more from zero during daytime, indicating that F_{O_2} estimates based on LE and water vapor profile and H and

695 temperature profile would lead to underestimation or overestimation, respectively, during daytime by the flux-gradient method (Fig. 6). The F_{O_2} estimates during nighttime were more uncertain based on temperature and water vapor, as indicated by large standard deviations. These "outliers" occurred due to too small vertical gradients, caused by a small activity of sources and sinks and/or of insufficient turbulence. The flux-gradient method based on CO_2 mole fractions and fluxes yielded F_{O_2} estimates in better agreement with modeled F_{O_2}. But this was probably because the O_2 sources and sinks were highly correlated to CO_2

700 processes due to the O_2 modeling set-up and constant ER (Eq. (1)). Consequently, it is still recommended to use all the available gas or energy gradients to derive O_2 fluxes with the flux-gradient methods, and then choose the most appropriate method (if this is possible) for various times during the day or year depending on the magnitude of the gradients, the quality of flux measurements and the turbulence. The magnitude of the gradients could additionally be increased for each scalar by choosing scalar-specific measurement heights.

705 The flux-gradient method has already been used for O_2 flux estimation above a cool temperate forest (Ishidoya et al., 2015), an urban canopy (Ishidoya et al., 2020) and a boreal forest (Faassen et al., 2022). The latter study applied a three-heights flux gradient approach, where they estimated the eddy diffusivity K based on CO_2 and temperature measurements at three heights and applied a vertical O_2 gradient between two heights. We also tested this three-heights flux gradient approach based on our model simulations, but we assumed that all scalars including O_2 were measured at three heights. Based on our simulations, we

710   could not observe an improvement of the flux estimation due to the inclusion of three measurement heights in the flux-gradient method instead of two heights.

Uncertainty on O_2 mole fraction estimates resulted in a median close to zero for the uncertainty $\sigma_{F_{O_2}}$. The uncertainty in O_2 mole fraction estimates were selected randomly following a normal distribution in the model simulations. Our analysis showed that the flux-gradient method has the potential for F_{O_2} estimation, but we also found that estimated F_{O_2} could be over- or

715   underestimated by up to ±5.5 $\mu mol\ m^{-2}\ s^{-1}$. To make the flux-gradient method more precise, the vertical scalar gradient should be as large as possible and flux and profile measurements as precise as possible. To achieve this, on the one hand, a larger distance between measurement heights is needed (not possible over large forest stands, but applicable for crop-, grass-, and peatland), and on the other hand, a higher measurement precision is necessary to reduce the uncertainty in scalar gradient measurements.

720   In general, mass is transported in air due to diffusive and non-diffusive processes. Diffusive transport can be induced due to random turbulent or molecular motions acting against a gradient. As shown in Figure 5, an exemplary vertical profile or gradient of CO_2 mole fraction regarding dry air shows a higher mole fraction close to the soil surface due to respiratory processes and a lower mole fraction within the forest canopy due to net assimilation during daytime. Above the canopy the CO_2 dry air mole fraction increases slightly again within the boundary layer. The vertical O_2 profile is mirrored to this CO_2

725   profile (when dry air mole fractions are considered). Because of the processes of evaporation and transpiration from the soil surface and canopy, water vapor is also added to the air column, where the vertical water vapor profile usually shows a decreasing water vapor mole fraction with increasing height. The addition of water vapor molecules to an air package dilutes the other molecules in that air package such as N_2, O_2 and CO_2 by replacing some of them. Thus, the ratio between number of O_2 or CO_2 molecules and total number of air molecules (= mole fraction regarding moist air) decreases and therefore the

730   vertical O_2 and CO_2 gradients change. Furthermore, due to the addition of water vapor molecules, other air molecules are being displaced and moved away from the evaporating surface. This displacement effect yields in a non-diffusive transport (also known as Stefan flow) that does not necessarily follow a gradient (Kowalski, 2017; Kowalski et al., 2021). The magnitudes of the dilution and displacement effects depend on the mass fraction of each gas (number and weight of molecules per mass of air), where O_2 is more affected than CO_2 due to its high abundance (Kowalski et al., 2021). Considering the above described

735   vertical profile, O_2 diffuses downwards towards the evaporating surface following the increased gradient due to the dilution effect. However, this downward motion can be offset by the displacement effect.

To analyze the transport of and the relationship between O_2 and CO_2 molecules, the dilution and displacement effects have to be considered - also in relation to the turbulent transport. The magnitudes and directions of diffusive (turbulence and molecular diffusion) and non-diffusive transport are variable and need to be quantified experimentally for various atmospheric conditions,

740   various ecosystems and heights above the ecosystems. Thus, the significance and impacts of the various transport types are unknown and currently under discussion. In regard to the many open questions towards non-diffusive transport, we have not implemented the Stefan flow within CANVEG until now.

The CANVEG model considers mole fractions regarding dry air (removing all the water vapor) for O_2 and CO_2, and therefore the dilution effect is excluded from the model simulations and vertical gradients do not change due to the process of evapotranspiration. This allows comparison to O_2 measurements where it is common practice to cryogenically dry the air before analysis for O_2 (Pickers et al., 2017). The non-diffusive transport (Stefan flow) would play a role in our study within the application of the flux-gradient method and the estimation of ER_{conc}. By the modification of the vertical gradients due to the non-diffusive transport, flux estimates based on the flux-gradient method would differ (personal communication with Andrew Kowalski). However, our study considered mostly net ecosystem fluxes in this application. Further, Kowalski et al. (2021) determined that the Webb, Pearman and Leuning (WPL) methodology, based on perturbations in the dry air mass fraction, correctly estimated biogeochemical fluxes (for both water vapor and CO_2) despite incorrectly describing transport mechanisms. Therefore, the WPL methodology predicts that artificially eliminating the effects of water vapor (dilution and displacement) and expressing each gas with reference to dry air will yield the equivalent flux-gradient relationships. Furthermore, by assuming all scalars (temperature, water vapor, CO_2 and O_2) are transported similarly (and thus assuming the eddy diffusivities K_o, K_c, K_T and K_v are the same), we have added an additional uncertainty. Also due to the change in the vertical gradients, the estimation of ER_{conc} will be affected, because the displacement by evapotranspiration has a different impact on CO_2 and O_2. However, again for the mole fractions regarding dry air, the effect should be small. Also, the estimated ER_{conc} (and also ER_{eco}) were reasonable and in line with current process understanding. Lastly, in our study, F_{CO_2} obtained with the eddy covariance technique was source partitioned based on simulated F_{O_2} and the uncertainty in gross assimilation (σ_{F_A}) was evaluated. By estimating CO_2 flux components following the same approach based on stable isotopes in CO_2, Knohl and Buchmann (2005) derived a σ_{F_A} for instantaneous half-hourly data of 6 µmol m^{-2} s^{-1} assuming CO_2 and $^{13}CO_2$ flux uncertainties of 0.5 µmol m^{-2} s^{-1} and 25‰ µmol m^{-2} s^{-1}, respectively. A σ_{F_A} of around 4 µmol m^{-2} s^{-1} was found with a higher uncertainty in CO_2 fluxes ($\sigma_{F_{CO_2}}$) = 2 µmol m^{-2} s^{-1} by Ogee et al. (2004). Our study obtained comparable results under similar $\sigma_{F_{CO_2}}$ = 2.5 µmol m^{-2} s^{-1} (Fig. 7b). However, Ogee et al. (2004) found that σ_{F_A} can be reduced to 2 µmol m^{-2} s^{-1} when an isotopic disequilibrium is larger than 0.004 (Fig. 6 in Ogee et al. (2004), page 11). We obtained ER_A and ER_R disequilibrium ($|ER_A - ER_R|$) of around 0.086 mol mol^{-1}, but still could not improve our σ_{F_A} under normal $\sigma_{F_{CO_2}}$ level (Fig. 7b). This was probably because our uncertainty in O_2 fluxes ($\sigma_{F_{O_2}}$) was much larger (up to 15 µmol m^{-2} s^{-1}) relative to the ER_A and ER_R disequilibrium (0.086 mol mol^{-1}) (Ogee et al., 2004). Here, we derived $\sigma_{F_{O_2}}$ based on the analysis of the flux-gradient application (Fig. 6d). Thus, a higher precision in F_{O_2} estimates and/or a larger ER_A and ER_R disequilibrium ≥ 0.086 mol mol^{-1} is needed. In our simulations, the disequilibrium had low variation due to the fixed ER parameters. A small variation was only introduced by the variable ER_{rd} due to leaf temperature. Implementing variable ER parameters (depending on environmental conditions etc.) in the model or obtaining real ER values by measurements could be beneficial. Figure 7c shows that by improving the precision in F_{CO_2} and ER_R estimates and not so much in F_{O_2} also yields a lower uncertainty in estimates of gross assimilation. Faassen et al. (2022) changed ER_{eco} by ±0.20 mol mol^{-1}, which resulted in a change in partitioned F_A of

775 6.7%. However, they compared their partitioned flux components with F_A and F_R derived using the eddy covariance method, by assuming that the latter describes the "true" values. They emphasize the importance of a correct estimate for ER_{eco}. Our evaluation of σ_{F_A} was based on assigned *a priori* uncertainties to all elements which were independent of the flux values (Ogee et al., 2004). Compared with eddy covariance data, our partitioned F_A also differed by about 6% which is comparable to flux partitioning results by Faassen et al. (2022).

5 Conclusions

We implemented $O_2{:}CO_2$ exchange ratios in the CANVEG multi-layer ecosystem-atmosphere gas exchange model to enable hourly ecosystem O_2 flux simulations. The simulated ecosystem $O_2{:}CO_2$ exchange ratio (ER_{eco}) showed strong diel and seasonal variations. The annual mean ER_{eco} ranged from 1.06 to 1.12 mol mol^{-1} during the five years' study period and depended significantly on our assumptions about the fixed model parameters describing the exchange ratios of the ecosystem

785 components: leaves, stem and soil (ER_A, ER_{stem}, ER_{soil}). Especially, changes in ER_{soil} by $\pm10\%$ yielded annual mean ER_{eco} from 1.00 up to 1.24 mol mol^{-1}. We also found that hourly ER_{eco} and exchange ratios of net assimilation (ER_{An}) exhibited high variability during transition periods (e.g., during sunrise and sunset) with low flux magnitudes.

According to our simulations, it is feasible to derive ecosystem O_2 fluxes with the flux-gradient approach based on sensible heat, latent heat and CO_2 turbulent flux measurements under field conditions, when the vertical gradients are measured between

790 1.05 to 2 times of the canopy height. Specially, the vertical O_2 difference should be larger than 1 ppm. However, including uncertainty in O_2 mole fraction measurements by 0.7 ppm would increase the uncertainty in O_2 flux estimates up to 15 μmol m^{-2} s^{-1}. The precision of the source partitioning application was driven by *a priori* uncertainties of O_2 and CO_2 flux, ER_A and ER_R measurements. With an ER_A and ER_R disequilibrium ($|ER_A - ER_R|$) of about 0.086 mol mol^{-1}, the uncertainty of partitioned gross assimilation can be constrained to < 5 μmol m^{-2} s^{-1} by narrowing the uncertainty of CO_2 measurements and ER_R estimates

795 to 2.5 μmol m^{-2} s^{-1} and 0.05 mol mol^{-1}. O_2 fluxes measurements and additional information on the exchange ratios of gross assimilation and ecosystem respiration (ER_A, ER_R), for example obtained by chamber measurements, can thus be used as a source partitioning approach for net CO_2 fluxes.

Our model study highlighted the potential temporal and spatially variability of $O_2{:}CO_2$ exchange ratios of various ecosystem components and the drivers of O_2 fluxes at a forest study site. Furthermore, we provided guidance to micrometeorological

800 approaches, such as the flux-gradient method, to obtain sufficient O_2 flux estimates depending on measurement set-up and on current instrument precision. We further tested the usage of O_2 flux estimates to source partition net CO_2 fluxes. Further understanding of the relationship between environmental drivers and O_2 fluxes and $O_2{:}CO_2$ exchange ratios, and continuous and long-term observations based on, for example, long term chamber measurements, will greatly help to improve our ecosystem model and our understanding of the carbon cycle in terrestrial ecosystems.

Code/Data availability

The data sets and model code generated and/or analyzed during the current study are available from the corresponding author.

Author contributions

YY and AKn designed the work. YY conducted the main analysis, and AKl and FM aided its interpretation. MC provided the model code. YY primarily wrote the paper with input from all coauthors.

Competing interests

The authors declare that they have no conflict of interest.

Acknowledgements

This research was funded by the European Research Council under the European Union's Horizon 2020 research and innovation program (grant agreement no. 682512–OXYFLUX). We acknowledge support by the Open Access Publication Funds of the Göttingen University. We thank the staff from the Bioclimatology Group of the University of Göttingen, especially Dietmar Fellert, Frank Tiedemann, Edgar Tunsch and Marek Peksa, for their continuous support in data acquisition and instrument maintenance. We thank Penelope A. Pickers, Emmanuel Blei, Julian Deventer and Mattia Bonazza for building O_2 measurement systems and providing atmospheric O_2 and CO_2 data. We also thank Jelka Braden-Behrens for obtaining leaf area measurements, Ashehad Ali for suggestions on model parameter calibrations, Jan Muhr for interpretations of ER results, and Rijan Tamrakar and Christian Markwitz for preparing the meteorological and eddy covariance data. Also, we thank the forest manager Ulrich Breitenstein for allowing the experimental setup at the Leinefelde site. We also thank Andrew S. Kowalski for his important input and suggestions regarding the process of non-diffusive transport during the open discussion. Finally, we thank the reviewers for their helpful and constructive comments that improved the quality of this paper.

Appendix A

Table A1. Nomenclature and abbreviations. [**] Units with m^{-2} indicate "per leaf area" (otherwise always "per ground area").

Abbreviation	Unit	Full name
ARQ	mol mol^{-1}	apparent respiratory quotient
b	μmol m^{-2} s^{-1} [**]	intercept of Ball-Berry model after Collatz et al. (1991)
CO_2 atm	ppm	atmospheric CO_2 mole fraction

c_p	J kg^{-1} K^{-1}	specific heat capacity of air
DOY		day of year
Equ_{O_2}	ppm	difference of O_2 mole fraction from 209750 ppm (derived as the intercept of the relationship between measured atmospheric O_2 and CO_2 mole fractions, cf. Table 1)
ER	mol mol^{-1}	O_2:CO_2 exchange ratio
ER_A	mol mol^{-1}	O_2:CO_2 exchange ratio of gross assimilation
ER_A^b	mol mol^{-1}	*a priori* mean of ER_A
ER_{An}	mol mol^{-1}	O_2:CO_2 exchange ratio of net assimilation
ER_{conc}	mol mol^{-1}	atmospheric O_2:CO_2 mole fraction ratio
ER^z_{conc}	mol mol^{-1}	height dependent atmospheric O_2:CO_2 mole fraction ratio
ER_{eco}	mol mol^{-1}	ecosystem O_2:CO_2 exchange ratio
ER^z_{eco}	mol mol^{-1}	height dependent ecosystem O_2:CO_2 exchange ratio
ER_R	mol mol^{-1}	O_2:CO_2 exchange ratio of ecosystem respiration
ER_R^b	mol mol^{-1}	*a priori* mean of ER_R
ER_{rd}	mol mol^{-1}	O_2:CO_2 exchange ratio of leaf dark respiration
ER_{soil}	mol mol^{-1}	O_2:CO_2 exchange ratio of soil respiration
ER_{stem}	mol mol^{-1}	O_2:CO_2 exchange ratio of stem respiration
F_A	μmol m^{-2} s^{-1}	gross assimilation CO_2 flux (gross carboxylation minus photorespiration)
F_A^b	μmol m^{-2} s^{-1}	*a priori* mean of F_A
F_{CO_2}	μmol m^{-2} s^{-1}	net ecosystem CO_2 flux
$F^z_{CO_2}$	μmol m^{-2} s^{-1}	height dependent net ecosystem CO_2 flux
$F_{\widetilde{CO_2}}$	μmol m^{-2} s^{-1}	net turbulent CO_2 flux
f_{DBH}		fraction of stem diameter to the diameter at breast height
f_{LAI}		fraction of LAI per layer
F_{O_2}	μmol m^{-2} s^{-1}	net ecosystem O_2 flux
$F^z_{O_2}$	μmol m^{-2} s^{-1}	height dependent net ecosystem O_2 flux
$F_{\widetilde{O_2}}$	μmol m^{-2} s^{-1}	net turbulent O_2 flux
F_R	μmol m^{-2} s^{-1}	gross ecosystem respiration CO_2 flux

F_R^b	$\mu mol\ m^{-2}\ s^{-1}$	*a priori* mean of F_R
F_{rd}	$\mu mol\ m^{-2}\ s^{-1}$	leaf dark respiration CO_2 flux
F_{soil}	$\mu mol\ m^{-2}\ s^{-1}$	soil respiration CO_2 flux
F_{stem}	$\mu mol\ m^{-2}\ s^{-1}$	stem respiration CO_2 flux
H	$W\ m^{-2}$	net ecosystem sensible heat flux
$\tilde{H}$	$W\ m^{-2}$	net turbulent sensible heat flux
ht	m	canopy height
J		cost function
J_{max25}	$\mu mol\ m^{-2}\ s^{-1}$	maximum electron transport rate at 25 °C
k_{ball}		slope of Ball-Berry model after Collatz et al. (1991)
K_c, K_o, K_T, K_v	$m^2\ s^{-1}$	eddy diffusivity of CO_2, O_2, heat and water vapor
LAI	$m^2\ m^{-2}$	leaf area index
LE	$W\ m^{-2}$	net ecosystem latent heat flux
$\tilde{LE}$	$W\ m^{-2}$	net turbulent latent heat flux
$leaf_{out}$		DOY for the start of leaf growth
$leaf_{full}$		DOY for the end of leaf growth
$leaf_{fall}$		DOY for the start of leaf fall
$leaf_{fall\_complete}$		DOY for the end of leaf fall
MCMC		Markov-Chain Monte Carlo methods
$O_{2\ atm}$	ppm	atmospheric O_2 mole fraction
OR		oxidative ratio
r_1, r_2		coefficients for exponential relationship between soil temperature and soil respiration
R_{d25}	$\mu mol\ m^{-2}\ s^{-1}$	leaf dark respiration at 25 °C
RMSE		root mean squared error
T	°C	air temperature
T_{leaf}	°C	leaf temperature
T_{optjm}	°C	optimum temperature for electron transport
T_{optvc}	°C	optimum temperature for maximum carboxylation
V_{cmax25}	$\mu mol\ m^{-2}\ s^{-1}$ [**]	maximum carboxylation at 25 °C

WAI	$m^2\,m^{-2}$	wood area index
z	m	height above the surface
α		fraction of the photosystem II activity
Δc	ppm	vertical CO_2 mole fraction difference
$\Delta F_{O_2,(c,T,v)}$	$\mu mol\,m^{-2}\,s^{-1}$	difference between O_2 fluxes derived by the flux-gradient method and by model simulations. The subscripts c, T and v represent the considered scalar profiles for CO_2 mole fraction, temperature and water vapor.
Δo	ppm	vertical O_2 mole fraction difference
ΔT	°C	vertical air temperature difference
Δv	$kg\,m^{-3}$	vertical water vapor density difference
Δz	m	vertical height difference
θ_J		curvature parameter of light response curve
λ	$J\,kg^{-1}$	latent heat of vaporization
ρ_m	$kg\,m^{-3}$	air mass density
ρ_n	$mol\,m^{-3}$	air molar density
σ_{ER_A}	$mol\,mol^{-1}$	*a posteriori* uncertainty of ER_A
$\sigma_{ER_A^b}$	$mol\,mol^{-1}$	*a priori* uncertainty of ER_A
σ_{ER_R}	$mol\,mol^{-1}$	*a posteriori* uncertainty of ER_R
$\sigma_{ER_R^b}$	$mol\,mol^{-1}$	*a priori* uncertainty of ER_R
σ_{F_A}	$\mu mol\,m^{-2}\,s^{-1}$	*a posteriori* uncertainty of F_A
$\sigma_{F_A^b}$	$\mu mol\,m^{-2}\,s^{-1}$	*a priori* uncertainty of F_A
$\sigma_{F_{CO_2}}$	$\mu mol\,m^{-2}\,s^{-1}$	uncertainty of CO_2 flux estimates
$\sigma_{F_{O_2}}$	$\mu mol\,m^{-2}\,s^{-1}$	uncertainty of O_2 flux estimates
σ_{F_R}	$\mu mol\,m^{-2}\,s^{-1}$	*a posteriori* uncertainty of F_R
$\sigma_{F_R^b}$	$\mu mol\,m^{-2}\,s^{-1}$	*a priori* uncertainty of F_R

References

830 Angert, A., Yakir, D., Rodeghiero, M., Preisler, Y., Davidson, E., and Weiner, T.: Using O_2 to study the relationships between soil CO_2 efflux and soil respiration, Biogeosciences, 12, 2089-2099, doi:10.5194/bg-12-2089-2015, 2015.

Angert, A., Muhr, J., Negron Juarez, R., Alegria Muñoz, W., Kraemer, G., Ramirez Santillan, J., Barkan, E., Mazeh, S., Chambers, J. Q., and Trumbore, S. E.: Internal respiration of Amazon tree stems greatly exceeds external CO_2 efflux, Biogeosciences, 9, 4979-4991, doi:10.5194/bg-9-4979-2012, 2012.

835 Anthoni, P. M., Knohl, A., Rebmann, C., Freibauer, A., Mund, M., Ziegler, W., Kolle, O., and Schulze, E. D.: Forest and agricultural land-use-dependent CO_2 exchange in Thuringia, Germany, Global Change Biol, 10, 2005-2019, doi:10.1111/j.1365-2486.2004.00863.x, 2004.

Baldocchi, D.: A Lagrangian random-walk model for simulating water vapor, CO_2 and sensible heat flux densities and scalar profiles over and within a soybean canopy, Bound-Lay Meteorol, 61, 113-144, doi:10.1007/BF02033998, 1992.

Baldocchi, D.: Measuring and modelling carbon dioxide and water vapour exchange over a temperate broad-leaved forest during the 1995 summer drought, Plant Cell Environ, 20, 1108-1122, doi:10.1046/j.1365-3040.1997.d01-147.x, 1997.

840 Baldocchi, D., Falge, E., Gu, L. H., Olson, R., Hollinger, D., Running, S., Anthoni, P., Bernhofer, C., Davis, K., Evans, R., Fuentes, J., Goldstein, A., Katul, G., Law, B., Lee, X. H., Malhi, Y., Meyers, T., Munger, W., Oechel, W., U, K. T. P., Pilegaard, K., Schmid, H. P., Valentini, R., Verma, S., Vesala, T., Wilson, K., and Wofsy, S.: FLUXNET: A new tool to study the temporal and spatial variability of ecosystem-scale carbon dioxide, water vapor, and energy flux densities, B Am Meteorol Soc, 82, 2415-2434, doi:10.1175/1520-0477(2001)082<2415:FANTTS>2.3.CO;2, 2001.

845 Baldocchi, D. D. and Wilson, K. B.: Modeling CO_2 and water vapor exchange of a temperate broadleaved forest across hourly to decadal time scales, Ecol Model, 142, 155-184, doi:10.1016/S0304-3800(01)00287-3, 2001.

Baldocchi, D. D., Hincks, B. B., and Meyers, T. P.: Measuring biosphere-atmosphere exchanges of biologically related gases with micrometeorological methods, Ecology, 69, 1331-1340, doi:10.2307/1941631, 1988.

Baldocchi, D. D., Wilson, K. B., and Gu, L. H.: How the environment, canopy structure and canopy physiological functioning influence
850 carbon, water and energy fluxes of a temperate broad-leaved deciduous forest-an assessment with the biophysical model CANOAK, Tree Physiology, 22, 1065-1077, doi:10.1093/treephys/22.15-16.1065, 2002.

Baldocchi, D. D., Fuentes, J. D., Bowling, D. R., Turnipseed, A. A., and Monson, R. K.: Scaling isoprene fluxes from leaves to canopies: Test cases over a boreal aspen and a mixed species temperate forest, J Appl Meteorol, 38, 885-898, doi:10.1175/1520-0450(1999)038<0885:SIFFLT>2.0.CO;2, 1999.

855 Battle, M., Bender, M. L., Tans, P. P., White, J. W. C., Ellis, J. T., Conway, T., and Francey, R. J.: Global carbon sinks and their variability inferred from atmospheric O_2 and delta ^{13}C, Science, 287, 2467-2470, 2000.

Battle, M. O., Munger, J. W., Conley, M., Sofen, E., Perry, R., Hart, R., Davis, Z., Scheckman, J., Woogerd, J., Graeter, K., Seekins, S., David, S., and Carpenter, J.: Atmospheric measurements of the terrestrial O_2:CO_2 exchange ratio of a midlatitude forest, Atmos Chem Phys, 19, 8687-8701, doi:10.5194/egusphere-egu22-4213, 2019.

860 Bowling, D. R., Tans, P. P., and Monson, R. K.: Partitioning net ecosystem carbon exchange with isotopic fluxes of CO_2, Global Change Biol, 7, 127-145, doi:10.1046/j.1365-2486.2001.00400.x, 2001.

Braden-Behrens, J., Markwitz, C., and Knohl, A.: Eddy covariance measurements of the dual-isotope composition of evapotranspiration, Agricultural and Forest Meteorology, 269, 203-219, doi:10.1016/j.agrformet.2019.01.035, 2019.

Braden-Behrens, J., Yan, Y., and Knohl, A.: A new instrument for stable isotope measurements of ^{13}C and [18]O in CO_2 – instrument
865 performance and ecological application of the Delta Ray IRIS analyzer, Atmos. Meas. Tech., 10, 4537-4560, 10.5194/amt-10-4537-2017, 2017.

Busch, F. A., Sage, R. F., and Farquhar, G. D.: Plants increase CO_2 uptake by assimilating nitrogen via the photorespiratory pathway, Nature Plants, 4, 46-54, doi:10.1038/s41477-017-0065-x, 2018.

Collatz, G. J., Ball, J. T., Grivet, C., and Berry, J. A.: Physiological and environmental-regulation of stomatal conductance, photosynthesis
870 and transpiration - a model that includes a laminar boundary-layer, Agricultural and Forest Meteorology, 54, 107-136, doi:10.1016/0168-1923(91)90002-8, 1991.

Emad, A. and Siebicke, L.: True eddy accumulation – Part 1: Solutions to the problem of non-vanishing mean vertical wind velocity, Atmos. Meas. Tech., 16, 29-40, 10.5194/amt-16-29-2023, 2023a.

Emad, A. and Siebicke, L.: True eddy accumulation – Part 2: Theory and experiment of the short-time eddy accumulation method, Atmos.
875 Meas. Tech., 16, 41-55, 10.5194/amt-16-41-2023, 2023b.

Faassen, K. A. P., Nguyen, L. N. T., Broekema, E. R., Kers, B. A. M., Mammarella, I., Vesala, T., Pickers, P. A., Manning, A. C., Vilà-Guerau de Arellano, J., Meijer, H. A. J., Peters, W., and Luijkx, I. T.: Diurnal variability of atmospheric O_2, CO_2 and their exchange ratio above a boreal forest in southern Finland, Atmos. Chem. Phys. Discuss., 2022, 1-33, 10.5194/acp-2022-504, 2022.

Farquhar, G. D., Caemmerer, S. V., and Berry, J. A.: A biochemical-model of photosynthetic CO_2 assimilation in leaves of C_3 species,
880 Planta, 149, 78-90, doi:10.1007/BF00386231, 1980.

Goulden, M. L., Munger, J. W., Fan, S. M., Daube, B. C., and Wofsy, S. C.: Measurements of carbon sequestration by long-term eddy covariance: Methods and a critical evaluation of accuracy, Global Change Biol, 2, 169-182, doi:10.1111/j.1365-2486.1996.tb00070.x, 1996.

Hanson, P. J., Amthor, J. S., Wullschleger, S. D., Wilson, K., Grant, R. F., Hartley, A., Hui, D., Hunt, J., E Raymond, Johnson, D. W., and Kimball, J. S.: Oak forest carbon and water simulations: model intercomparisons and evaluations against independent data, Ecological
885 Monographs, 74, 443-489, doi:10.1890/03-4049, 2004.

Helm, J., Hartmann, H., Göbel, M., Hilman, B., Herrera Ramírez, D., and Muhr, J.: Low-cost chamber design for simultaneous CO_2 and O_2 flux measurements between tree stems and the atmosphere, Tree Physiology, 41, 1767-1780, doi:10.1093/treephys/tpab022, 2021.

Hicks Pries, C., Angert, A., Castanha, C., Hilman, B., and Torn, M. S.: Using respiration quotients to track changing sources of soil respiration seasonally and with experimental warming, Biogeosciences, 17, 3045-3055, doi:10.5194/bg-17-3045-2020, 2020.

890 Hilman, B. and Angert, A.: Measuring the ratio of CO_2 efflux to O_2 influx in tree stem respiration, Tree Physiology, 36, 1422-1431, doi:10.1093/treephys/tpw057, 2016.

Hilman, B., Weiner, T., Haran, T., Masiello, C. A., Gao, X., and Angert, A.: The apparent respiratory quotient of soils and tree stems and the processes that control It, Journal of Geophysical Research: Biogeosciences, 127, e2021JG006676, doi:10.1029/2021JG006676, 2022.

Hilman, B., Muhr, J., Trumbore, S. E., Kunert, N., Carbone, M. S., Yuval, P., Wright, S. J., Moreno, G., Pérez-Priego, O., Migliavacca, M.,
895 Carrara, A., Grünzweig, J. M., Osem, Y., Weiner, T., and Angert, A.: Comparison of CO_2 and O_2 fluxes demonstrate retention of respired CO_2 in tree stems from a range of tree species, Biogeosciences, 16, 177-191, doi:10.5194/bg-16-177-2019, 2019.

Hockaday, W. C., Gallagher, M. E., Masiello, C. A., Baldock, J. A., Iversen, C. M., and Norby, R. J.: Forest soil carbon oxidation state and oxidative ratio responses to elevated CO_2, J Geophys Res-Biogeo, 120, 1797-1811, doi:10.1002/2015JG003010, 2015.

Ishidoya, S., Murayama, S., Kondo, H., Saigusa, N., Kishimoto-Mo, A. W., and Yamamoto, S.: Observation of O_2:CO_2 exchange ratio for
900 net turbulent fluxes and its application to forest carbon cycles, Ecol Res, 30, 225-234, doi:10.1007/s11284-014-1241-3, 2015.

Ishidoya, S., Morimoto, S., Aoki, S., Taguchi, S., Goto, D., Murayama, S., and Nakazawa, T.: Oceanic and terrestrial biospheric CO_2 uptake estimated from atmospheric potential oxygen observed at Ny-Alesund, Svalbard, and Syowa, Antarctica, Tellus B, 64, 2012.

Ishidoya, S., Sugawara, H., Terao, Y., Kaneyasu, N., Aoki, N., Tsuboi, K., and Kondo, H.: O_2:CO_2 exchange ratio for net turbulent flux observed in an urban area of Tokyo, Japan, and its application to an evaluation of anthropogenic CO_2 emissions, Atmos Chem Phys, 20,
905 5293-5308, doi:10.5194/acp-20-5293-2020, 2020.

Ishidoya, S., Murayama, S., Takamura, C., Kondo, H., Saigusa, N., Goto, D., Morimoto, S., Aoki, N., Aoki, S., and Nakazawa, T.: O_2:CO_2 exchange ratios observed in a cool temperate deciduous forest ecosystem of central Japan, Tellus B, 65, doi:10.3402/tellusb.v65i0.21120, 2013.

Juergensen, J., Muhr, J., and Knohl, A.: Variations of the oxidative ratio across ecosystem components and seasons in a managed temperate
910 beech forest (Leinefelde, Germany), Forests, 12, 2021.

Keeling, R. F. and Manning, A. C.: 5.15 - Studies of Recent Changes in Atmospheric O_2 Content, in: Treatise on Geochemistry (Second Edition), edited by: Holland, H. D., and Turekian, K. K., Elsevier, Oxford, 385-404, doi:10.1016/B978-0-08-095975-7.00420-4, 2014.

Keeling, R. F. and Shertz, S. R.: Seasonal and interannual variations in atmospheric oxygen and implications for the global carbon-cycle, Nature, 358, 723-727, 1992a.

915 Keeling, R. F. and Shertz, S. R.: Seasonal and interannual variations in atmospheric oxygen and implications for the global carbon cycle, Nature, 358, 723-727, doi:10.1038/358723a0, 1992b.

Knohl, A. and Baldocchi, D. D.: Effects of diffuse radiation on canopy gas exchange processes in a forest ecosystem, J Geophys Res-Biogeo, 113, doi:10.1029/2007JG000663, 2008.

Knohl, A. and Buchmann, N.: Partitioning the net CO_2 flux of a deciduous forest into respiration and assimilation using stable carbon
920 isotopes, Global Biogeochem Cy, 19, doi:10.1029/2004GB002301, 2005.

Kowalski, A. S.: The boundary condition for vertical velocity and its interdependence with surface gas exchange, Atmos. Chem. Phys., 17, 8177-8187, 10.5194/acp-17-8177-2017, 2017.

Kowalski, A. S., Serrano-Ortiz, P., Miranda-García, G., and Fratini, G.: Disentangling turbulent gas diffusion from non-diffusive transport in the boundary layer, Bound-Lay Meteorol, 179, 347-367, 10.1007/s10546-021-00605-5, 2021.

925 Krogh, A.: The Composition of the Atmosphere: An Account of Preliminary Investigations and a Programme, v. 1, no. 12, A.F. Høst1919.

Lenschow, D. H., Mann, J., and Kristensen, L.: How long is long enough when measuring fluxes and other turbulence statistics, J Atmos Ocean Tech, 11, 661-673, doi:10.1175/1520-0426(1994)011<0661:HLILEW>2.0.CO;2, 1994.

Manning, A. C. and Keeling, R. F.: Global oceanic and land biotic carbon sinks from the Scripps atmospheric oxygen flask sampling network, Tellus B, 58, 95-116, doi:10.1111/j.1600-0889.2006.00175.x, 2006.

930 Meredith, L., Commane, R., Munger, J., Dunn, A., Tang, J., Wofsy, S., and Prinn, R.: Ecosystem fluxes of hydrogen: a comparison of flux-gradient methods, Atmos Meas Tech, 7, 2787-2805, doi:10.5194/amt-7-2787-2014, 2014.

Ogee, J., Peylin, P., Cuntz, M., Bariac, T., Brunet, Y., Berbigier, P., Richard, P., and Ciais, P.: Partitioning net ecosystem carbon exchange into net assimilation and respiration with canopy-scale isotopic measurements: An error propagation analysis with $^{13}CO_2$ and $CO^{18}O$ data, Global Biogeochem Cy, 18, doi:10.1029/2003GB002166, 2004.

935 Oikawa, P. Y., Sturtevant, C., Knox, S. H., Verfaillie, J., Huang, Y. W., and Baldocchi, D. D.: Revisiting the partitioning of net ecosystem exchange of CO_2 into photosynthesis and respiration with simultaneous flux measurements of $^{13}CO_2$ and CO_2, soil respiration and a biophysical model, CANVEG, Agricultural and Forest Meteorology, 234-235, 149-163, doi:10.1016/j.agrformet.2016.12.016, 2017.

Pickers, P. A., Manning, A. C., Sturges, W. T., Le Quéré, C., Mikaloff Fletcher, S. E., Wilson, P. A., and Etchells, A. J.: In situ measurements of atmospheric O_2 and CO_2 reveal an unexpected O_2 signal over the tropical Atlantic Ocean, Global Biogeochem Cy, 31, 1289-1305,
940 doi:10.1002/2017GB005631, 2017.

Randerson, J., Masiello, C., Still, C., Rahn, T., Poorter, H., and Field, C.: Is carbon within the global terrestrial biosphere becoming more oxidized? Implications for trends in atmospheric O_2, Global Change Biol, 12, 260-271, doi:10.1111/j.1365-2486.2006.01099.x, 2006.

Raupach, M. R.: Applying Lagrangian fluid mechanics to infer scalar source distributions from concentration profiles in plant canopies, Agricultural and Forest Meteorology, 47, 85-108, doi:10.1016/0168-1923(89)90089-0, 1989.

945   Rebmann, C., Aubinet, M., Schmid, H., Arriga, N., Aurela, M., Burba, G., Clement, R., De Ligne, A., Fratini, G., Gielen, B., Grace, J., Graf, A., Gross, P., Haapanala, S., Herbst, M., Hortnagl, L., Ibrom, A., Joly, L., Kljun, N., Kolle, O., Kowalski, A., Lindroth, A., Loustau, D., Mammarella, I., Mauder, M., Merbold, L., Metzger, S., Molder, M., Montagnani, L., Papale, D., Pavelka, M., Peichl, M., Roland, M., Serrano-Ortiz, P., Siebicke, L., Steinbrecher, R., Tuovinen, J. P., Vesala, T., Wohlfahrt, G., and Franz, D.: ICOS eddy covariance flux-station site setup: a review, Int Agrophys, 32, 471-+, doi:10.1515/intag-2017-0044, 2018.

950   Schober, R.: Ausbauchungsreihen, Grundner, F., Schwappach, A, 1952.

Seibt, U., Brand, W. A., Heimann, M., Lloyd, J., Severinghaus, J. P., and Wingate, L.: Observations of O_2:CO_2 exchange ratios during ecosystem gas exchange, Global Biogeochem Cy, 18, doi:10.1029/2004GB002242, 2004.

Severinghaus, J.: Studies of the Terrestrial O_2 and Carbon Cycles in Sand Dune Gases and in Biosphere 2, Dissertation, doi:10.2172/477735, 1995.

955   Stephens, B. B., Keeling, R. F., and Paplawsky, W. J.: Shipboard measurements of atmospheric oxygen using a vacuum-ultraviolet absorption technique, Tellus B: Chemical and Physical Meteorology, 55, 857-878, doi:10.3402/tellusb.v55i4.16386, 2003.

Tamrakar, R., Rayment, M. B., Moyano, F., Mund, M., and Knohl, A.: Implications of structural diversity for seasonal and annual carbon dioxide fluxes in two temperate deciduous forests, Agricultural and Forest Meteorology, 263, 465-476, doi:10.1016/j.agrformet.2018.08.027, 2018.

960   Tarantola, A.: Inverse Problem Theory and Methods for Model Parameter Estimation, Society for Industrial and Applied Mathematics, doi:10.1137/1.9780898717921, 2004.

Tcherkez, G., Nogues, S., Bleton, J., Cornic, G., Badeck, F., and Ghashghaie, J.: Metabolic origin of carbon isotope composition of leaf dark-respired CO_2 in French bean, Plant Physiol, 131, 237-244, doi:10.1104/pp.013078, 2003.

Tohjima, Y., Mukai, H., Machida, T., Hoshina, Y., and Nakaoka, S. I.: Global carbon budgets estimated from atmospheric O_2/N_2 and CO_2
965   observations in the western Pacific region over a 15-year period, Atmos Chem Phys, 19, 9269-9285, 2019.

Van Oijen, M., Rougier, J., and Smith, R.: Bayesian calibration of process-based forest models: bridging the gap between models and data, Tree Physiology, 25, 915-927, doi:10.1093/treephys/25.7.915, 2005.

Wehr, R. and Saleska, S. R.: An improved isotopic method for partitioning net ecosystem-atmosphere CO_2 exchange, Agricultural and Forest Meteorology, 214, 515-531, doi:10.1016/j.agrformet.2015.09.009, 2015.

970   Wilson, J.: Turbulent transport within the plant canopy, 1989.

Worrall, F., Clay, G. D., Masiello, C. A., and Mynheer, G.: Estimating the oxidative ratio of the global terrestrial biosphere carbon, Biogeochemistry, 115, 23-32, doi:10.1007/s10533-013-9877-6, 2013.

Yakir, D. and Wang, X. F.: Fluxes of CO_2 and water between terrestrial vegetation and the atmosphere estimated from isotope measurements, Nature, 380, 515-517, doi:10.1038/380515a0, 1996.

975   Zobitz, J. M., Burns, S. P., Ogee, J., Reichstein, M., and Bowling, R.: Partitioning net ecosystem exchange of CO_2: A comparison of a Bayesian/isotope approach to environmental regression methods, J Geophys Res-Biogeo, 112, doi:10.1029/2006JG000282, 2007.